Title

A MEASUREMENT OF THE DIFFERENTIAL CROSS SECTIOSN FOR CHARGE EXCHANGE AND RADIATIVE CAPTURE OF NEGATIVE PIONS IN HYDROGEN AT 50 MeV LABORATORY ENERGY

Author

Carroll, Jim B.

Publication Date

1967-04-01

UCRL-11697

University of California

Ernest O. Lawrence Radiation Laboratory

A MEASUREMENT OF THE DIFFERENTIAL CROSS SECTIONS FOR CHARGE EXCHANGE AND RADIATIVE CAPTURE OF NEGATIVE PIONS IN HYDROGEN AT 50 MeV LABORATORY ENERGY

Berkeley, California

DISCLAIMER

Research and Development

UCRL-11697

UNIVERSITY OF CALIFORNIA

Lawrence Radiation Laboratory
Berkeley, California

AEC Contract No. W-7405-eng-48

A MEASUREMENT OF THE DIFFERENTIAL CROSS SECTIONS FOR CHARGE EXCHANGE AND RADIATIVE CAPTURE OF NEGATIVE PIONS IN HYDROGEN AT 50 MeV LABORATORY ENERGY

Jim B. Carroll

(Ph. D. Thesis)

April 1967

Contents

A MEASUREMENT OF THE DIFFERENTIAL CROSS SECTIONS FOR CHARGE EXCHANGE AND RADIATIVE CAPTURE OF NEGATIVE PIONS IN HYDROGEN AT 50 MeV LABORATORY ENERGY

Jim B. Carroll

Lawrence Radiation Laboratory
University of California
Berkeley, California

April 1967

ABSTRACT

The differential cross sections of

$$\pi^- + p \rightarrow \gamma + n$$

and

$$\pi^- + p \rightarrow \pi^0 + n \; (\rightarrow \gamma + \gamma + n)$$

have been measured at an incident pion laboratory-system kinetic energy of 54 MeV. The reactions were identified by detecting and measuring the energy of a final-state photon with a large total absorption counter placed at a laboratory-system angle of 84 deg. Analysis of the photon energy spectrum yields the center-of-mass differential cross section for the first reaction, $d\sigma_1/d\Omega^* \; (\theta^* = 90 \text{ deg}) = 51.5 \pm 10.7$ μb/sr, and the coefficients of the Legendre expansion of the center-of-mass system differential cross section for the second reaction,

$$d\sigma_2(\theta^*)/d\Omega^* = \sum_{\ell=0}^{2} A_\ell P_\ell (\cos \theta^*),$$

where $A_0 = 0.68 \pm 0.04$ mb/sr, $A_2 = 0.53 \pm 0.09$ mb/sr, and A_1 is not determined.

Using the principle of detailed balance, and our measurement of the cross section for the first reaction, we have calculated the isotropic term in the cross section for the reaction $\gamma + n \rightarrow \pi^- + p$, obtaining $a_0^- = 15.4 \pm 3.2$ μb/sr at $p_\gamma^* = 170$ MeV/c. This value is in reasonable agreement with other data obtained from photoproduction in deuterium.

I. INTRODUCTION

There has been considerable discussion in recent years about some apparent difficulties with the parameters of low-energy pion physics. These parameters come from the cross sections for pion-nucleon scattering at low energy, from the Panofsky ratio, and from the cross sections for pion photoproduction near threshold. It has been known[1] since 1952 that it should be possible to relate these parameters to each other by using the principles of detailed balance and charge independence and some assumptions about the energy dependences of the cross sections.

The expression relating the measurable quantities may be obtained in the following way. The principle of detailed balance states,[2] for the reactions of interest,

$$\sigma_{\pi^- p \to \gamma n}(E) = 2(k/q)^2 \, \sigma_{\gamma n \to \pi^- p}(E). \qquad (1)$$

In the above expression σ indicates a center-of-mass system (c.m.) cross section in which the initial state is unpolarized and in which no spins are measured in the final state. The cross sections are to be measured at the same total c.m. energy, E. The c.m. momentum of the pion is represented by q, and k represents the c.m. momentum of the photon.

The Panofsky ratio may be defined as

$$P = \frac{\omega(\pi^- p \to \pi^0 n)}{\omega(\pi^- p \to \gamma n)} ,$$

where ω indicates a transition rate for pions stopped in hydrogen. Because at low energies only S waves contribute to the cross section, and since the capture process is believed to proceed from S states only, we may write

$$P = \lim_{Q \to 0} \frac{\sigma_{\pi^- p \to \pi^0 n}(Q)}{\sigma_{\pi^- p \to \gamma n}(Q)} , \qquad (2)$$

where Q is the total kinetic energy in the c.m. The substitution is permissible because the relation between the transition probability and the cross section is the same for both processes.

Combining expressions 1 and 2, we obtain

$$\sigma_{\pi^- p \to \pi^0 n}(Q \to 0) = 2(k/q)^2 P \sigma_{\gamma n \to \pi^- p}(Q \to 0). \qquad (3)$$

This is the basic connection between the Panofsky ratio and the cross sections for charge exchange and π^- photoproduction. There are two reasons why expression 3, in itself, is of no practical use. In the first place, it is impossible to measure the cross sections at Q = 0, and in the second place, measurement of the π^- photoproduction cross section is not possible because of lack of a free neutron target. The second difficulty may be overcome by using deuterium as a target and applying corrections to account for the presence of the extra nucleon in the initial and final states. Measured cross sections may then be extrapolated to Q = 0 by using theoretically predicted energy dependences. Thus, in practice, a comparison of the relevant data through expression 3 is a test of (a) the deuterium-to-free-neutron correction, (b) the theoretical energy dependences, and (c) the principle of detailed balance.

Both the charge-exchange and photoproduction cross sections vary rapidly with energy for values of Q near zero. Most of this variation is due to phase-space factors which are customarily removed. In the following we assume that Q is small, and that only S waves are present.

The charge-exchange cross section may be written

$$\sigma_{cx} = \frac{8\pi}{9} \frac{v_0}{v_-} \left(\frac{\delta_1 - \delta_3}{q} \right)^2 ,$$

where v_0 and v_- are the c.m. velocities of the π^0 and π^- respectively; q is the c.m. momentum of the π^-; and δ_1 is the S-wave phase shift corresponding to a state with total isospin 1/2. (As in the rest of the thesis, we use units such that $\hbar = c = 1$.) Or, in terms of the scattering lengths,

$$a = \lim_{q \to 0} \frac{\delta}{q} ,$$

$$\sigma_{cx}(Q \to 0) = \frac{8\pi}{9} \frac{v_0}{v_-} (a_1 - a_3)^2 . \qquad (4)$$

The cross section for photoproduction of π^+ from protons, or of π^- from neutrons, may be written

$$\sigma^{\pm} (Q \to 0) = \frac{4 \pi \epsilon q}{m^2 (1 + k/M)(1 + q/M)} a_0^{\pm} , \qquad (5)$$

where the superscript $\pm$ refers to the charge of the pion in the final state, and

ϵ = total c.m. energy of the pion,

q = c.m. momentum of the pion,

k = c.m. momentum of the photon,

m = pion mass,

M = nucleon mass.

Combining expressions 3, 4, and 5, and performing the necessary arithmetic, one obtains

$$(a_1 - a_3)_{cx} = 3.820 \sqrt{P a_0^-} . \qquad (6)$$

The subscript, cx, is meant to emphasize that the principle of charge independence has not been used explicitly. The introduction of isospin states (and implicitly the principle of charge independence) in expression 4 is not strictly necessary. One could introduce the charge-exchange data into expression 3 by using a "charge-exchange scattering length," a_{cx}, provided that one had theoretical means for extrapolating the data to Q = 0. By using the principle of charge independence one may compare the value of $(a_1 - a_3)$ obtained from charge-exchange data alone with that calculated from elastic scattering data.

In 1958, Puppi[3] discussed a set of data indicating a large disagreement between the value of $(a_1 - a_3)$ obtained from charged pion-nucleon scattering data and the value obtained from an expression

similar to 6. At that time it was necessary to obtain the π^- photoproduction cross section from the relation

$$\sigma_{\gamma n \to \pi^- p} = \frac{\sigma_{\gamma n \to \pi^- p}}{\sigma_{\gamma p \to \pi^+ n}} \sigma_{\gamma p \to \pi^+ n},$$

where the minus-to-plus ratio

$$R_{-/+} = \frac{\sigma_{\gamma n \to \pi^- p}}{\sigma_{\gamma p \to \pi^+ n}}$$

was obtained from measurements of the similar quantity in deuterium,

$$R^d = \frac{\sigma_{\gamma d \to \pi^- pp}}{\sigma_{\gamma d \to \pi^+ nn}},$$

using Baldin's corrections[4] to account for the presence of the extra nucleon. The set of data

$$R_{-/+} = 1.34 \pm 0.14 \quad \text{(from Ref. 3)},$$

$$P = 1.50 \pm 0.11 \quad \text{(Ref. 5)},$$

and $\sigma_{\gamma p \to \pi^+ n} = (1.43 \pm 0.06)\ q \cdot 10^{-28}\ \text{cm}^2$ (Ref. 6)

yielded

$$a_1 - a_3 = 0.209 \pm 0.028,$$

while analysis of charged pion-nucleon scattering gave

$$a_1 - a_3 = 0.27 \pm 0.02 \quad \text{(Ref. 7)}.$$

Subsequent theoretical investigations indicated several errors in the above analysis. Cini et al.[8] noted that the methods used in extrapolating both the phase shifts and the photoproduction data were incorrect. They suggested that the scattering lengths be obtained from an extrapolation based on dispersion theory, and that the extrapolation of the photoproduction data be revised to include the effects of the retardation term. These points were discussed further in the paper of Hamilton and Woolcock,[9] who also noted the necessity for applying an

additional Coulomb correction to the phase shifts. These corrections brought the experimental data into agreement with expression 6. In a later paper, Hamilton and Woolcock concluded[10] that the data were consistent not only with expression 6 but also with several other relations imposed upon the phase shifts by dispersion relations. Recent evaluations of new experimental data have again raised the question of whether the data are consistent with expression 6. These recent data are discussed further in Sec. V.

The chain of arguments, calculations, and corrections which connects the deuterium data to the charge-exchange data is a lengthy one. It was the purpose of this experiment to shorten the unsupported length of the chain by providing a measurement at an intermediate step--specifically, a measurement of the cross section for the radiative capture reaction $\pi^- + p \rightarrow \gamma + n$. A measurement of this cross section would permit comparison with the photoproduction data through the detailed balance calculation and the deuterium corrections without any extrapolation to $Q = 0$. If the measurement were done in such a way that the S-wave component could be isolated, and the results extrapolated to $Q = 0$, then comparison with the charge-exchange data could be made through the Panofsky ratio. In this way it might be possible to localize any inconsistency as belonging to one specific half of the chain of arguments, and to establish the accuracy of the other half.

II. EXPERIMENT

In this experiment we have measured the differential cross section for the radiative capture reaction $\pi^- + p \rightarrow \gamma + n$ at a c.m. angle of 90 deg and an incident pion laboratory-system (lab) kinetic energy of 54 MeV. (In the remainder of the thesis the radiative capture reaction will be referred to as reaction 1.) This was done by directing a measured flux of π^- mesons through a liquid hydrogen target and counting with high efficiency the high-energy photons produced at a lab angle of 84 deg (corresponding to $\theta_{c.m.} \approx 90$ deg). The energy spectrum of these photons was measured with a total-absorption scintillation counter, making it possible to distinguish between the monoenergetic photons ($E_\gamma = 170$ MeV) from reaction 1 and the larger number of photons which result from charge exchange,

$$\pi^- + p \rightarrow n + \pi^0 \xrightarrow[\tau \approx 10^{-15}\ \text{sec}]{} n + \gamma + \gamma ,$$

and which have energies E_γ within a band from 31 to 147 MeV. (The charge-exchange reaction will be referred to as reaction 2.) Our analysis also yields the angular distribution of π^0's produced in reaction 2.

A. Apparatus

A plan view of the experimental arrangement is shown in Fig. 1.

1. Pion Beam

A beam of negative particles (produced in an internal beryllium target by the circulating proton beam of the 184-inch cyclotron) was externally degraded, momentum analyzed, and focused onto the hydrogen target. Figure 2 is a schematic representation of the optical properties of the beam transport system. The momentum of the beam at the center of the target was determined to be 134 MeV/c by a differential range technique in which the final absorber was the liquid hydrogen and its container. Although no attempt was made to unfold the range curve, its width was consistent with a momentum spread of $\pm 6\%$ as calculated from the geometry of the arrangement and the properties of

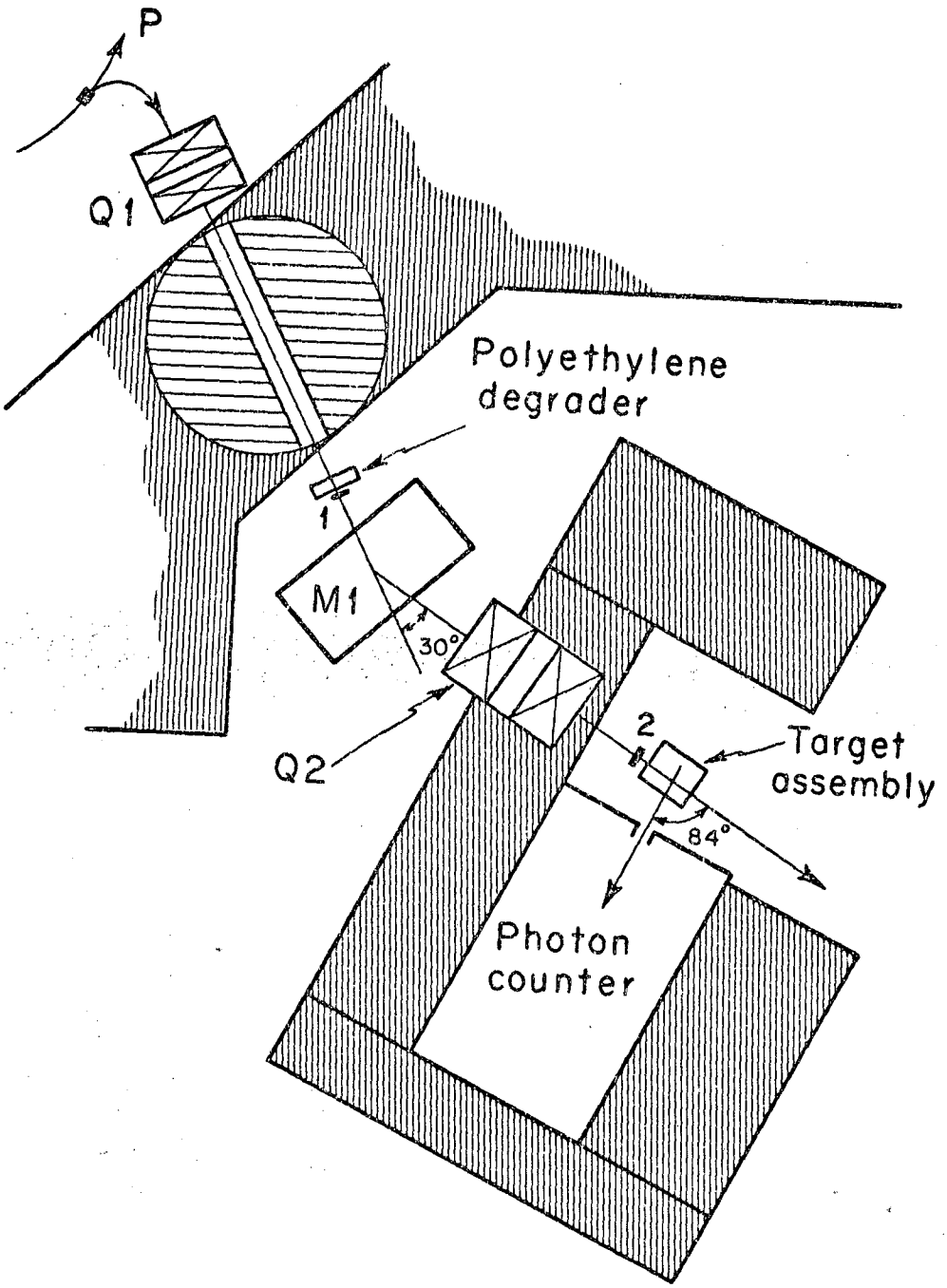

Fig. 1. Plan view of the experimental arrangement. Q_1 and Q_2 are doublet quadrupoles, M_1 is a bending magnet, and 1 and 2 are scintillation counters. Details of the photon counter and target assembly are shown in Fig. 4.

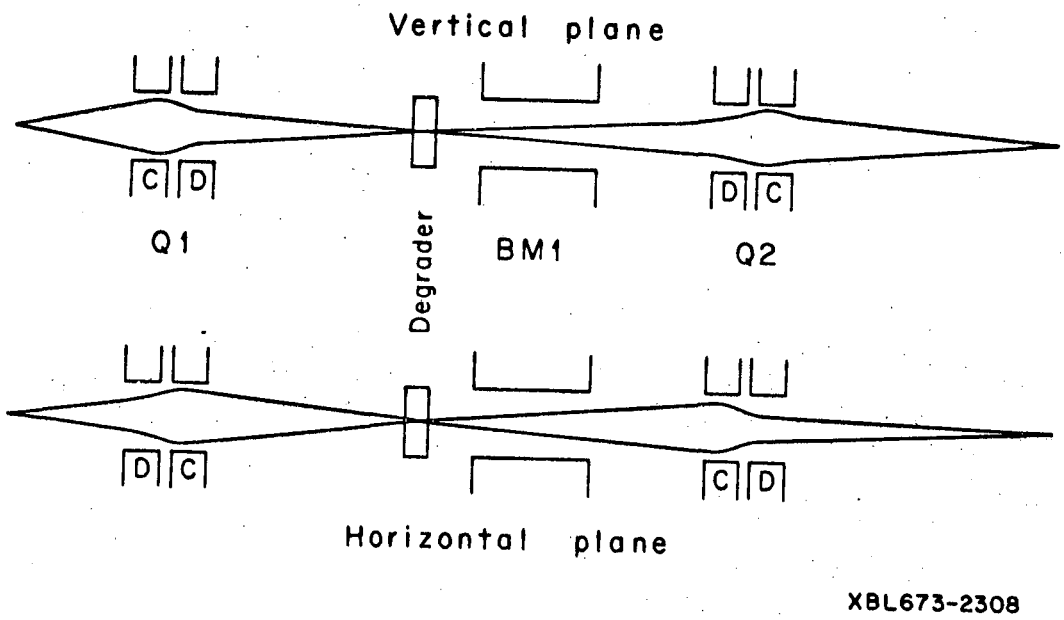

Fig. 2. Schematic representation of the optical properties of the beam transport system. For convenience only the deviations from the central ray are shown.

the magnets used.[11] The composition of the beam was determined by using a fast tunnel diode coincidence circuit[12] to measure the spectrum of particle time of flight between counters 1 and 2. Particles included in the spectrum were required by the electronics to meet the criteria imposed on the incident beam during the cross-section measurements. A typical spectrum is shown in Fig. 3. The relative numbers of particles in the pion, muon, and electron peaks were calculated by using a least-squares procedure to fit the data with a sum of three Gaussians. From the number of particles in the pion peak was subtracted the number of instances in which the decay $\pi \rightarrow \mu + \nu$ occurred with the μ passing through the second counter. Since the probability of this circumstance was significant only for decays occurring near counter 2, and since the velocities of the pion and the decay muon were not very different, these events all had flight times approximately equal to that of a pion. The true number of pions passing through the last counter was calculated to be $(90 \pm 1)\%$ of the number of particles included in the pion peak. The number of pions decaying between the last counter and the target was negligible. The beam composition was measured several times during the experiment; the average pionic fraction (including the above correction) was $F_\pi = 0.67 \pm 0.01$. The average pion flux through the final counter (3.5 in. high $\times$ 2.75 in. wide) was about 1.3×10^6 pions/min. The distribution of pion intensity in a plane perpendicular to the beam was measured at the location of the target with a 3/8-in.-diameter scintillator. It was required that particles included in this distribution have pion time of flight and fulfill the criteria for incident beam particles. The cyclotron auxiliary dee was used to provide a long beam spill, in which about half of the total flux was distributed over a period of 8.0 msec, the remainder being concentrated in an initial spike which was gated out electronically.

2. Hydrogen Target

The liquid hydrogen was contained in a Mylar flask supported in a vacuum by its fill and vent lines. The flask walls consisted of two layers of 0.075-in. Mylar bonded with an epoxy resin. The portions of the fill and vent lines near the flask were also Mylar. The profile of

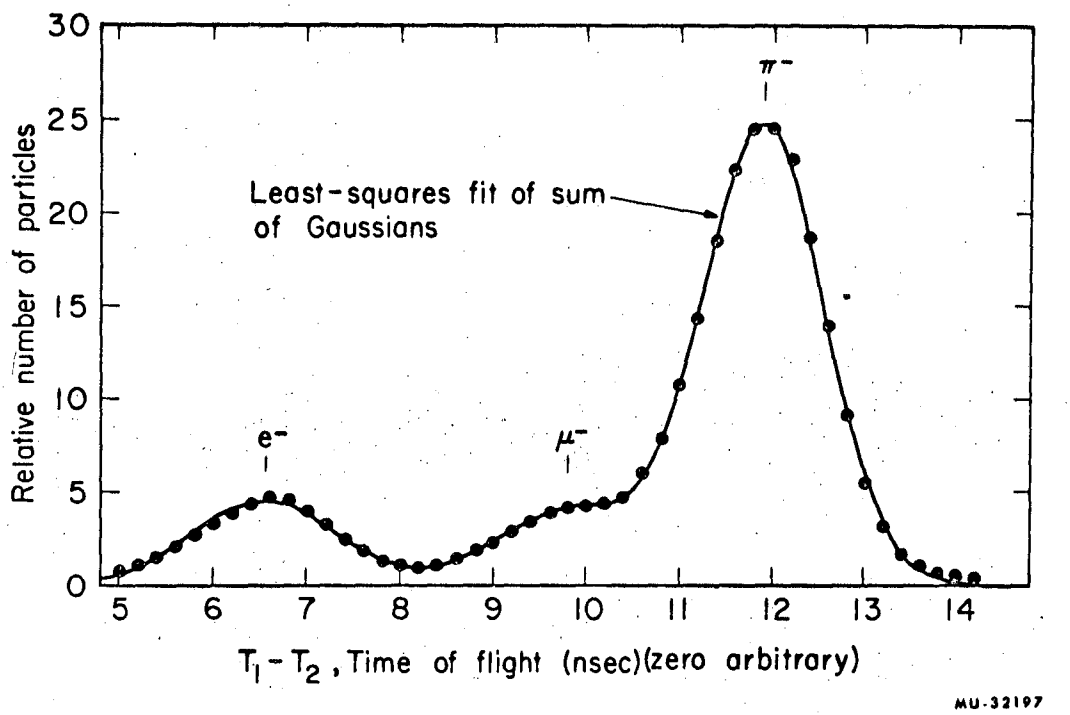

Fig. 3. A typical spectrum of particle flight time between counters 1 and 2. Statistical errors are smaller than the size of the points. The smooth curve represents the best fit to the data, assuming a Gaussian shape for each peak.

the flask (which was a figure of revolution about an axis parallel to the beam) is indicated in Fig. 4. Measurements of the profile were made with a traveling microscope with the flask filled with liquid nitrogen and suspended in a vacuum. The diameter of the flask was 5.0 in. and the thickness at the center was 3.0 in. Radiation shielding was provided by seven layers of 0.00025-in. doubly aluminized Mylar foil loosely wrapped about the flask, and by the scintillation counters surrounding the flask. The windows in the vacuum jacket for incoming and outgoing pions and for the outgoing photons consisted of three layers of 0.0075-in. Mylar and two layers of 0.001-in. Al foil.

3. Scintillation Counters

a. The monitor telescope

The positions of counters 1 and 2 are indicated in Fig. 1; other counters are shown in the enlarged view of the area near the target, Fig. 4. Each counter consisted of a piece of plastic scintillator attached by a Lucite coupling to a photomultiplier tube. Counters 1, 2, D, and 3 in coincidence were used to monitor the incident beam. In addition, counters 1 and 2 were used to measure the beam composition, as described in Sec. II. A. 1; counter D measured the dE/dx of each beam particle; counter 3 defined the size of the beam near the target. Counters 4A and 4B and 4C were used to detect charged particles emerging from the target.

b. The total-absorption photon counter

The total-absorption counter[13] was designed to detect photons with energies between 20 and 200 MeV with high efficiency and good energy resolution. It consisted of a cylinder of plastic scintillator 16 in. in diameter and 80 in. long in which the incident photon was converted into an electron-positron shower which subsequently deposited most of its energy in the scintillator. Estimates based on data of Kantz and Hofstadter[14] indicated that this configuration should contain, on the average, 94% of the incident photon energy.

The energy deposited in the counter was determined by measuring the amount of light produced in the scintillator. To obtain good energy resolution this light must be collected with an efficiency that is

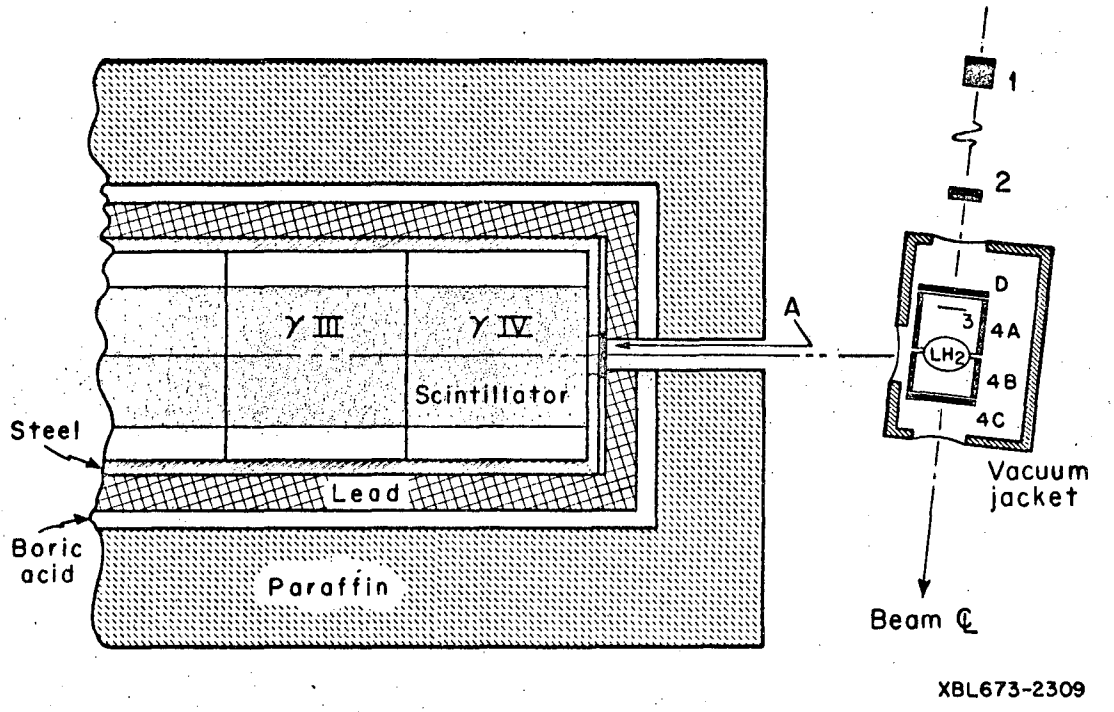

Fig. 4. Schematic section through photon counter and target assembly, showing scintillation counters surrounding the target and the arrangement of shielding around the photon counter.

insensitive to the location of the shower. This was accomplished by dividing the cylinder into four 20-in. sections; the surface of each section was covered with a diffusely reflecting coating (finely powdered alpha alumina in a binder of liquid polystyrene), and the light within each section was detected in six 2-in. -diameter photomultipliers (6655A) connected to the cylinder by Lucite light pipes (see Fig. 5). The anodes of the photomultipliers in each section were tied directly together with short cables. The high voltage of each photomultiplier was adjusted to equalize the gains of the tubes on each section. The light produced by minimum-ionizing cosmic rays passing coaxially through the section was used as a reference standard for this purpose. During the experiment the photomultiplier high voltages were maintained to ± 1 volt, and current-regulated dc light sources (1B59) mounted on each section were used to check the gain stability of the photomultipliers. Tests on the individual sections indicated that the position sensitivity was small (maximum variation with radius ≤ 5%) and that the energy resolution for charged particles was probably determined by the statistics of the number of photons collected by the photomultipliers. After the gains of the individual tubes were adjusted the relative gain of each section as a whole was measured by use of the cosmic ray reference standard mentioned above. The rise time of the pulse from the six tubes of one section was about 20 nsec, the fall time about 70 nsec, and the total pulse duration about 110 nsec.

The photon counter was shielded from the large neutron flux found near the cyclotron by surrounding it with the following materials: 1.5 in. iron, 4 in. lead, 2 in. compressed boric acid, and 14 in. paraffin (listed from inside to outside). A 3-7/8-in. -diameter circular coaxial opening in one end of the shielding defined the entrance aperture for the photons (Fig. 4). Counter A, placed between the photon counter and the opening in the shielding, was used to veto the cases in which a charged particle entered the photon counter through the aperture. The experimental area itself, which included the target and the photon counter, was shielded on the sides by about 5 ft of heavy concrete, and by 1 ft of iron above and below. With the shielding configuration as

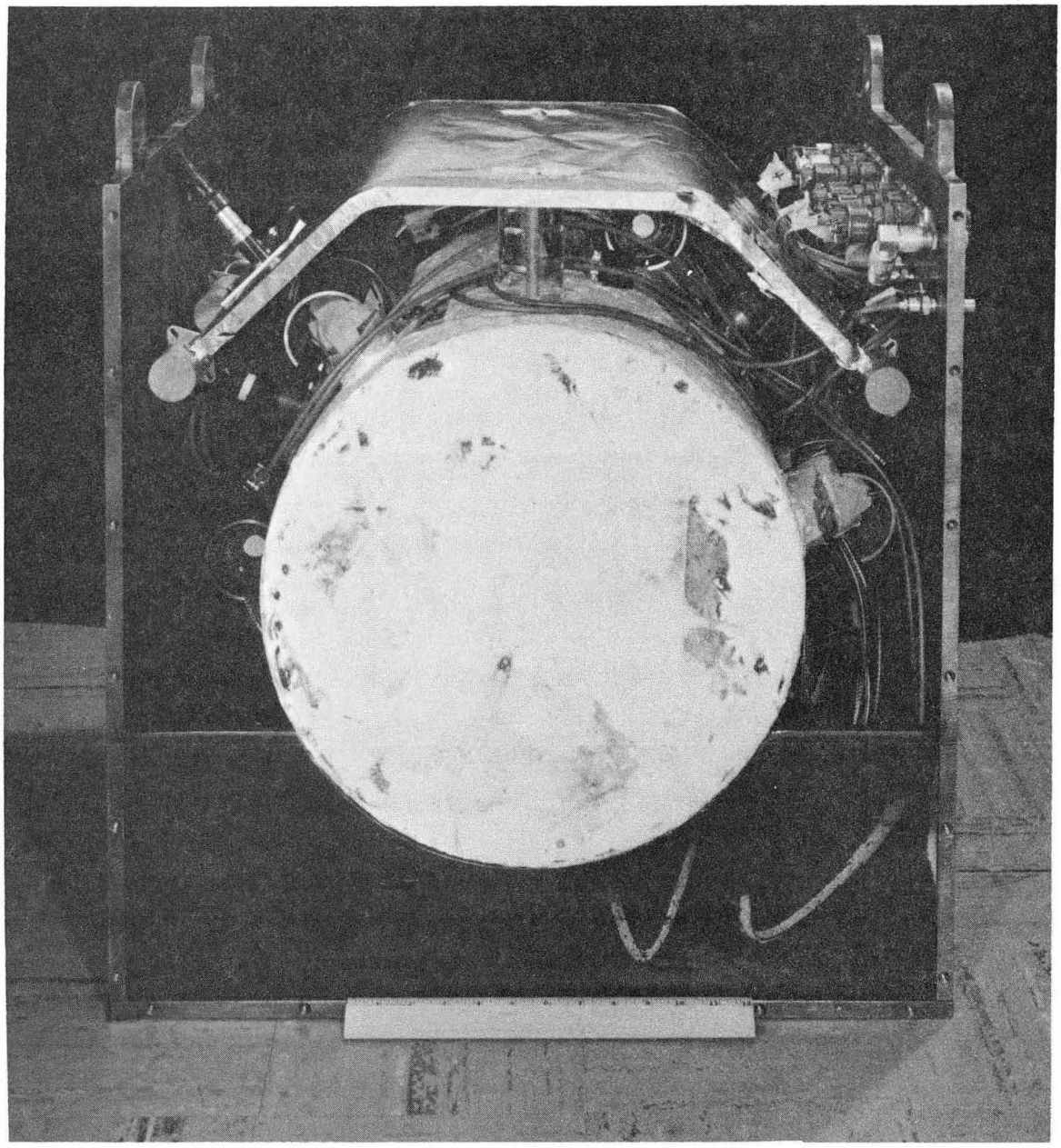

Fig. 5. Partially assembled section of photon counter, showing arrangement of phototubes and "umbrella" counter.

described, there were two sources of background counting rate in the photon counter: energetic cosmic rays, and neutrons associated with the cyclotron. The counting rate due to cosmic rays was about 120 per sec; the energy spectrum associated with these particles had a peak at about 80 MeV, and extended to energies greater than 200 MeV. This counting rate was reduced to about 60 per sec by placing a large veto counter just above each section of the photon counter (Fig. 5). Each of these counters (called U for umbrella) consisted of a sheet of plastic scintillator viewed from the edges by six 7117 photomultipliers. The signals from these tubes were added and placed into anticoincidence with the signal from the photon counter. With the full pion beam passing through the target, and with the signals from counters U and A placed in anticoincidence, the singles counting rate in the photon counter (i.e., no coincidence with the incident beam) was about 500 per sec. The energy spectrum obtained under these conditions decreased approximately exponentially with energy. Above about 80 MeV, the contribution from the machine-associated background was about equal to that from the cosmic rays. The determination of the energy calibration and the resolution of the counter are discussed in the section on data analysis.

4. Electronics

The electronics in this experiment had two basic functions: to count the number of incident particles, and to measure the pulse-height spectrum produced in the photon counter by photons from reactions 1 and 2. As a practical matter these operations were divided into three steps:

(a) Define and count the incident beam.

(b) Detect those events in which a pulse in the photon counter had the proper time correlation with a neutral interaction in the target.

(c) Measure the pulse-height from the photon counter for those events defined by (b).

Two partially independent methods of performing these operations were used. In one method, a multichannel pulse-height analyzer was used to record the pulse-height spectrum. To reduce the number of background counts included in the spectrum the criteria imposed by

the electronics for accepting a pulse for analysis were made as strict as possible without introducing bias into the spectrum. In the other method, the signals from all the counters in the experiment were displayed on a four-beam oscilloscope and were photographed. A photograph was taken if an event met either of two sets of criteria. One set was the same as that used in selecting events for the pulse-height analyzer. In the second set the coincidence requirement specified in (b) was weakened. A neon light was photographed concurrently with the signals, and an overall shift of the pulse locations indicated on the film which set of criteria were applicable. The film contained a great deal more correlated information about each event than could be obtained from the electronics, and was useful for checking for correct operation of the electronic part of the system.

A block diagram of the electronics is shown in Fig. 6. Not shown on the diagram is the alternative trigger arrangement for the four-beam oscilloscope which duplicated the coincidence required in C_4 but which had a longer coincidence-resolving time.

a. Logic

The incident beam was defined by the coincidence $C_2(1D3\overline{D^*3^*})$. (The * indicates a signal greater than some assigned threshold; the $\overline{\quad}$ indicates anticoincidence.) The $\overline{D^*}$ requirement eliminated incident particles with low velocity (as indicated by large dE/dx in D) which could stop in the liquid hydrogen. This was necessary because a stopped pion has a much larger probability of producing a photon (or photons) than an in-flight pion. (All stopped pions interact by reaction 1 or reaction 2; in our target fewer than 1% of the in-flight pions interacted through these channels.) Furthermore, the photon energy spectrum produced by stopping pions is very different from that produced by interactions occurring in flight. Thus a small fraction of stopping pions would cause appreciable distortion of the observed energy spectrum. The threshold for $\overline{D^*}$ was adjusted while the pulse-height spectrum from D was observed in a pulse-height analyzer which was gated on by the C_2 coincidence. The threshold was set to be slightly higher than the mean pulse height produced by pions with the average beam

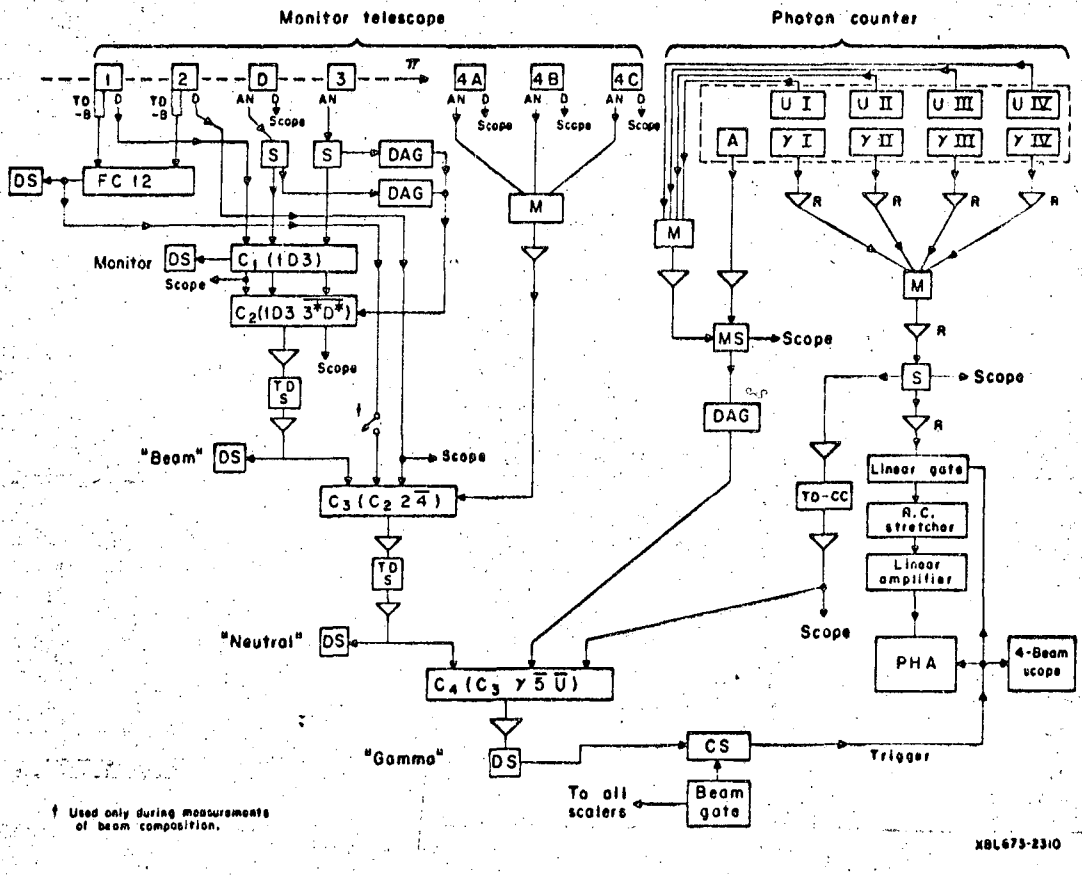

Fig. 6. Block diagram of electronics. Symbols are listed in Table I.

Table I. Symbols used in block diagram of electronics.

AN	Anode	
D	Dynode	
DS	Discriminator-scaler	
TD-B	Tunnel diode discriminator--Bjerke	See Ref. 12
FC	Fast coincidence	See Ref. 12
S	Splitter	
DAG	Delay and gate	
TD-S	Tunnel diode discriminator--Swift ($\approx$ 5 μsec pulse width)	
M	Mixer	
MS	Mixer-splitter	
∇	Hewlett-Packard 460-AR or 460 BR	
∇_R	Indicates B+ supply is external regulated supply	
TD-CC	Tunnel diode discriminator--Cordon Kerns (see Fig. 7)	
C	Coincidence circuit, Wenzel type	
CS	Slow dc coincidence circuit	

Unless otherwise noted, the equipment used here is described in the UCRL Counting Handbook.

momentum. Particles giving large pulses in counter 3 were rejected ($\overline{3^*}$) because this was found to improve the efficiency with which non-interacting beam particles could, in a subsequent coincidence, be vetoed by the counters surrounding the target.

Neutral interactions of the incident beam were detected by $C_3(C_2 2\overline{4})$. Here "4" represents the summed signals from 4A, 4B, and 4C--the counters surrounding the target. The coincidence with 2 was found to increase the efficiency for rejecting charged final states. The inefficiency of the anticoincidence arrangement, as measured by the ratio C_3/C_2, was 0.024. Thus, by requiring that C_3, rather than C_2, be in coincidence with the photon counter signal, the number of accidental counts included in the photon spectrum was reduced by a factor of 40.

The number of accidental counts may be decreased further by insuring that the resolving time used in detecting coincidences between neutral interactions (C_3) and pulses from the photon counter (γ) is as short as possible. This minimum resolving time was determined primarily by the requirement that it be large enough to include any time shifts due to the amplitude variations of the photon-counter signal. This is necessary if the photon energy spectrum is not to be distorted by an energy-dependent method of gating the pulse-height analyzer. This time-amplitude correlation was minimized by using a tunnel diode discriminator to detect the zero-crossing point of the differentiated photon counter pulse. The characteristics of this circuit (Fig. 7) were designed specifically to match the characteristics of the signal from the photon counter.[15] Thus, in spite of a pulse rise time of 20 nsec and an amplitude variation of (5.7/1), it was possible to achieve a resolution time of 5 nsec. (This represents the full width of the distribution of $T_2 - T_{\gamma d}$ as measured on the photographs of the oscilloscope traces. Here T indicates the time corresponding to the half height of the leading edge of a pulse, and 2 and γd indicate the signals from counter 2 and the special tunnel diode circuit, respectively.) To be conservative the coincidence resolving time used in $C_4(C_3\gamma\overline{AU})$, the coincidence which triggered the pulse-height analyzer during the experiment, was 20 nsec. As mentioned previously, $\overline{A}$ was used to reject

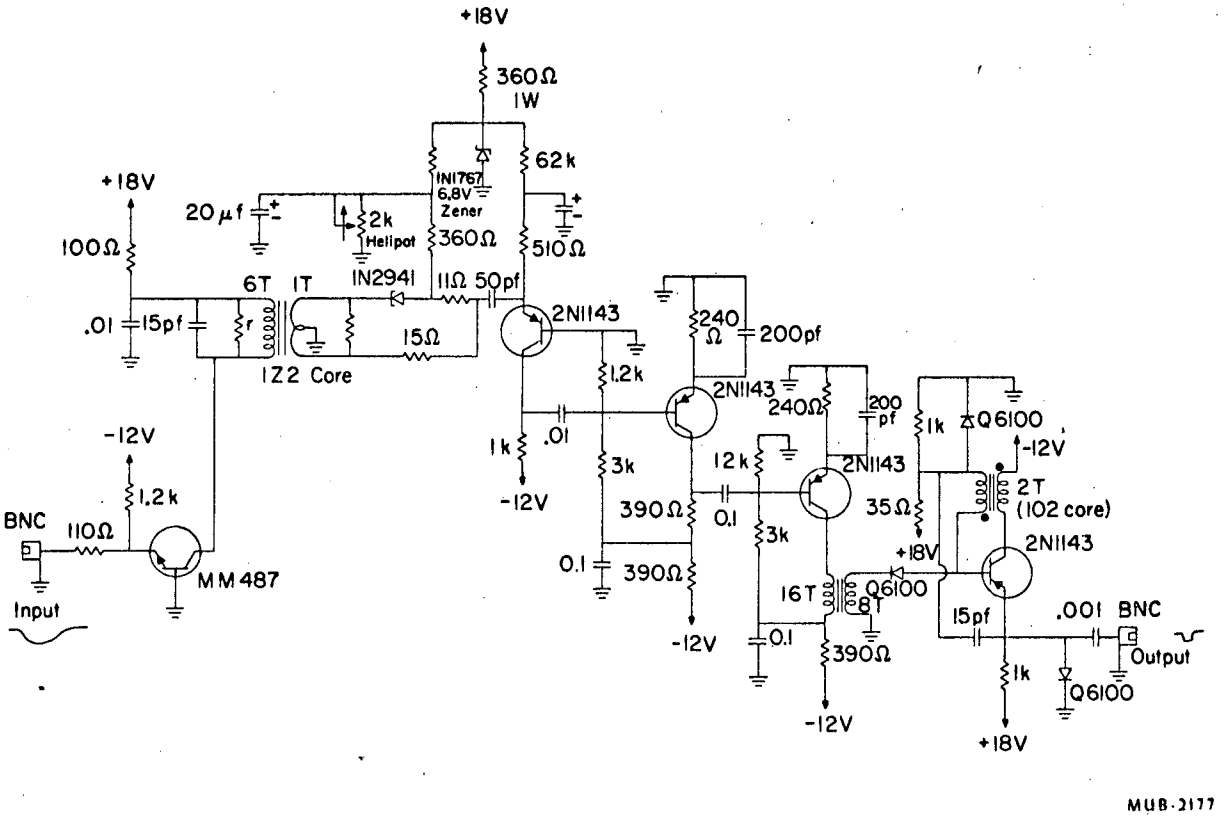

Fig. 7. Schematic diagram of the tunnel diode discriminator (TD-CC), which was used to improve the timing characteristics of the signal from the photon counter.

charged particles scattering into the photon counter through the aperture in the shielding, and $\bar{U}$ rejected about half the energetic cosmic rays passing through the counter.

In measuring the beam composition, coincidence C_3 was changed to $C_3(C_2 2F)$, where F represents the output of the fast coincidence FC(12). The counting rate in C_3 was then measured as a function of the relative delay of signals 1 and 2 at the input of FC. These measurements thus defined the relative composition of those beam particles satisfying the coincidence $(C_2 2)$. Coincidence $C_1(1D3)$ was used as a general monitor of the total flux and was also useful as a check for consistent operation of the rest of the electronics.

All scalers, and the C_4 output that triggered the pulse-height analyzer and the four-beam oscilloscope, were gated on by a master gate which was adjusted to exclude the initial spike in the cyclotron beam spill.

b. Pulse-height analysis

Amplifiers were used to compensate for the slight differences in response of the individual sections of the photon counter. The compensated signals were added and the sum signal was amplified and then split to provide signals for the pulse-height analyzer, the four-beam oscilloscope, and the timing circuitry. The signal for the pulse-height analyzer was amplified and passed through a linear gate which, when triggered by the output of C_4, was open for 0.5 μsec. The output of the linear gate was shaped by a passive RC circuit, amplified, and presented to the input of a RIDL pulse-height analyzer. Fast amplifiers (Hewlett-Packard 460-AR) were used for the photon signal in order to preserve timing information and so that the gate open time could be kept short to reduce the probability of pulse pile-up. In those amplifiers required to preserve pulse-height information the internal B^+ power supply was disconnected and replaced by an external regulated supply. Although this modification considerably improved their gain stability, these amplifiers were still the major source of drift in the pulse-height analysis portion of the electronics. The gain and the linearity of the electronics were measured by use of a precision pulser.

c. Four-beam oscilloscope

The signals to be photographed were amplified and delayed so that they presented a convenient display (Fig. 8). Also photographed simultaneously with the traces displaying the signals were an illuminated register giving the number of the picture, and a neon light which indicated in a binary fashion which of the two trigger modes mentioned at the beginning of Sec. II. A had caused the picture to be taken. The triggering of the oscilloscope was arranged so that the trigger signal representing the more stringent set of criteria always arrived earlier than that representing the looser criteria. Hence the location of pulses on the photograph was the same if the event causing the picture to be taken met either the strict criteria only, or both the strict and loose criteria; if, however, only the loose criteria were met, an overall shift of the pulses occurred because of the different triggering time. Where amplitude information was important (D and γ), the response of the oscilloscope system was calibrated by use of a precision pulser. The sweep speeds of the individual traces were calibrated by recording the output of an accurate radio-frequency generator. The sweep was nominally 20 nsec/cm.

B. Experimental Procedures

During the experiment both target-full and target-empty data were taken at 54 MeV. To minimize the statistical error in the subtracted data, the ratio of total incident flux (target full/target empty) was adjusted to be approximately equal to the square root of the ratio of the counting rates (target full/target empty) in the high-energy channels of the pulse-height analyzer. The duration of a typical run was 1 to 2 hours. In addition to the data from the scalers and the pulse-height analyzer, the run number, the elapsed time, and the initial and final frame numbers photographed by the oscilloscope camera were recorded for each run.

The known photon spectrum produced by stopping pions was used to provide an absolute calibration for the entire system. This calibration was performed several times during the experiment by

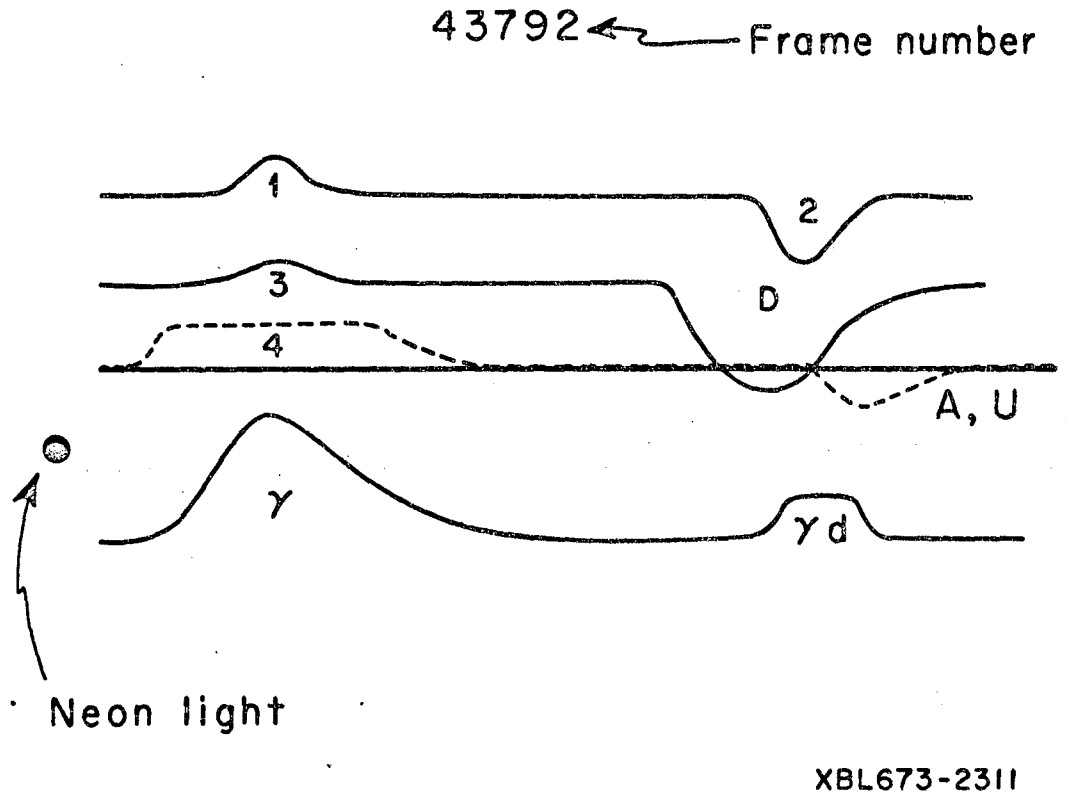

Fig. 8. Sketch showing the information recorded on the pictures of the four-beam oscilloscope. The pulse from the zero-crossing discriminator is labeled γd; other pulses are from scintillation counters indicated by the labels.

degrading the energy of the beam with absorbers, and removing the low-velocity anticoincidence requirement ($\overline{D}^*$) from C_2. The stopping pion rate was about 10^5 per min, and the calibration runs required about 15 to 30 min.

Several measurements of the beam composition were made during each period of continuous operation. The variation of the measured fractional number of pions was of the same order as the accuracy of the measurement, about ± 1%.

The gain of the pulse-height analysis system was measured frequently with a precision electrical pulser, and was readjusted when necessary. Changes in gain occurring during the collection of data rarely exceeded 1%. The gains of the individual sections of the photon counter were measured at the beginning of each period of operation, using the dc light sources as reference standards. With the photomultiplier high voltages maintained to ± 1 volt, the change in gain of the individual sections was found to be less than ± 0.5%.

III. DATA ANALYSIS

A. Pulse-Height Analyzer Spectrum

The object of the experiment was to measure the differential cross sections from Eqs. 1 and 2 (defined in Sec. II). In relating these cross sections to the experimental data, the double-differential cross section, $d^2\sigma_\gamma/d\Omega dk$, of photons in the laboratory system (lab) may be expressed in terms of the center-of-mass cross sections 1 and 2. By folding the double-differential cross section with the overall response function of the experimental apparatus, a calculated pulse-height spectrum is obtained. This calculated pulse-height spectrum is then compared with the one obtained experimentally, and the parameters describing cross sections 1 and 2 are adjusted to give a best fit in the sense of minimum χ^2.

The lab double-differential cross section of photons from reaction 1 may be written

$$\frac{d^2\sigma_{\gamma,1}}{d\Omega dk}(\theta, k, p) = \frac{d\sigma_{\gamma,1}}{d\Omega^*}(\theta^*, p^*)\frac{d\Omega^*}{d\Omega}\delta[k - k_1(\theta, p)]. \qquad (7)$$

Here $k_1(\theta, p)$ indicates the unique lab photon energy determined by the two-body kinematics, and δ is the Kronecker delta. (Other notations used in this section are defined in Table II.)

The c.m. differential cross section of π^0's from reaction 2 may be written in a Legendre series, as

$$\frac{d\sigma_{\pi^0,2}}{d\Omega^*_{\pi^0}}(\theta^*_{\pi^0}, p^*) = \sum_{j=0}^{j_{max}} A_j(p^*)P_j(\cos\theta^*_{\pi^0}). \qquad (8)$$

The coefficients of the Legendre series can then be used to describe the lab double-differential cross section of photons resulting from the decay of these π^0's (a derivation of this procedure may be found in Ref. 16):

Table II. Definition of notation.

*	indicates quantity in (π^- + p) center of mass
$\sigma_{\gamma, 1}$	cross section for γ's produced in reaction 1
$\sigma_{\pi^0, 2}$	cross section for π^0's produced in reaction 2
$\sigma_{\gamma, 2}$	cross section for γ's produced in reaction 2
Ω	solid angle of γ's, unless otherwise noted
θ	angle of γ's with respect to incident π^-, unless otherwise noted
k	energy of photon
p	momentum of incident π^-
β_0	velocity of π^0 in (π^- + p) center of mass, c = 1
g_0	$1/\sqrt{1 - \beta_0^2}$
m_0	rest mass of π^0
β	velocity of (π^- + p) center of mass in laboratory system
g	$1/\sqrt{1 - \beta^2}$

All quantities given in laboratory system unless otherwise noted.

$$\frac{d^2\sigma_{\gamma,2}}{d\Omega dk}(\theta, k, p) = B \sum_{j=0}^{j_{max}} A_j(p^*)P_j(X)P_j(Y), \qquad (9)$$

where

$$B = 2/\beta_0 g_0 m_0 g(1 - \beta\cos\theta),$$
$$X = (\cos\theta - \beta)/(1 - \beta\cos\theta) = \cos\theta^*,$$
$$Y = \frac{1}{\beta_0}\left[1 - \frac{m_0}{2g_0 g\, k\,(1 - \beta\cos\theta)}\right].$$

Here Y is the cosine of the angle between the detected photon and the π^0 which emitted it, evaluated in the $(\pi^- + p)$ center of mass.

Combining 7 and 9, we obtain the double-differential cross section describing the production of photons from both reactions:

$$\frac{d^2\sigma_\gamma}{d\Omega dk}(\theta, k, p) = B \sum_{j=0}^{j_{max}} A_j(p^*)P_j(X)P_j(Y) \qquad (10)$$

$$+ \frac{d\sigma_{\gamma,1}}{d\Omega^*}(\theta^*, p^*)\,\frac{d\Omega^*}{d\Omega}(\theta, p)\,\delta[k - k_1(\theta, p)].$$

We calculate the expected experimental pulse-height spectrum by folding this double-differential cross section with the characteristics of the measuring technique. The number of photons produced in the target with energy k, and within the solid angle defined by the aperture in the shielding of the photon counter, is obtained by folding together the double-differential cross section, the target thickness, the spatial and momentum distributions of the pion flux, and the solid angle subtended by the aperture at points within the target. After the integrations over all variables but θ and p (which determine the double-differential cross section) have been performed, the result may be expressed as

$$\frac{dN_\gamma}{dk}(k) = \rho N_\pi \iint g(p)W(\theta)\,\frac{d^2\sigma}{d\Omega dk}(\theta, k, p)\,d\theta dp. \qquad (11)$$

Here ρ is the density of the liquid hydrogen; N_π is the number of incident pions; and g(p) is the normalized distribution of incident pion momentum, p. $W(\theta)$ is the weighting factor (target thickness $\times$ solid angle) obtained as a result of the integrations. The integrations indicated in Eq. 11 are over $0 \leq p \leq \infty$ and $0 \leq \theta \leq \pi$, with contributions to the integral coming only from those regions where g(p) and $W(\theta)$ are nonzero. The integrations necessary to calculate $W(\theta)$ were performed numerically by a computer program.

The calculated distribution of counts in the pulse-height analyzer is then

$$N_i = \int_0^\infty \frac{dN_\gamma}{dk}(k)\, R(k, i)dk, \qquad (12)$$

where N_i denotes the number of counts in the ith channel, and R(k, i) is the overall response function of the photon counter and electronics. By combining Eqs. 11 and 12 we obtain

$$N_i = \rho N_\pi \iiint R(k, i)g(p)W(\theta)\frac{d^2\sigma_\gamma}{d\Omega dk}(\theta, k, p)d\theta dk dp. \qquad (13)$$

Expanding $d^2\sigma_\gamma/d\Omega dk$ into the individual terms of Eq. 10, we obtain

$$N_i = \rho N_\pi \epsilon \left[A_0 I_0(i) + A_1 I_1(i) + A_2 I_2(i) + \frac{d\sigma_{\gamma,1}}{d\Omega^*}(\theta^* = 90 \text{ deg}) I_3(i)\right], \qquad (14)$$

where

$$\epsilon I_j(i) = \iiint R(k, i)g(p)W(\theta)P_j(X)P_j(Y)d\theta dk dp \quad (\text{for } j = 0, 1, 2), \qquad (15)$$

$$\epsilon I_3(i) = \iiint R(k, i)g(p)W(\theta)\delta[k - k_1(\theta, p)]\, d\theta dk dp, \qquad (16)$$

ϵ is the energy-independent efficiency of the apparatus (electronic dead-time effects, etc.),

$I_0 \cdots I_3$ are the channel-number distributions obtained by folding the photon energy spectra described by the individual terms of Eq. 10 with response of the experimental apparatus.

In passing from Eq. 10 to Eq. 14, j_{max} has been made equal to 2 because, at the energy of this experiment, only orbital angular momentum states with $l = 0$ or 1 are expected to be important. Also, the explicit dependence on p of $d\sigma_{\gamma, 1}/d\Omega^*$ and A_j has been removed to indicate that these quantities now represent averages over the momenta present in the incident beam.

The response function must be known before the terms $(I_0 \cdots I_3)$ can be evaluated explicitly. We write the overall response function as a fold of three factors,

$$R(k, i) = \int\int R_1(k, L) R_2(L, V) R_3(V, i) dL dV,$$

where R_1 describes the transformation by the photon counter of photon energy k into scintillation light L; R_2 describes the transformation of scintillation light into an electrical pulse of amplitude V by the photomultiplier tubes on the photon counter; R_3 describes the transformation by the electronics of the electrical pulse of amplitude V into a count in channel i of the pulse-height analyzer.

Each of the response functions R(X, Y) gives the probability of obtaining an output Y from an input X.

The response of the photon counter, $R_1(k, L)$, was calculated by using a computer program to simulate by Monte Carlo techniques the development of the photon-electron-positron shower in the scintillator. The amount of energy deposited in the counter by ionization loss was then calculated from the path lengths of the electrons and positrons, and the amount of light produced in the scintillator was assumed to be proportional to this energy loss. Two independent calculations of $R_1(k, L)$ were made, by use of programs developed by Poirier[17] and by Zerby.[18] The results of these calculations for an incident photon energy of 150 MeV are shown in Fig. 9.

The photomultiplier response was assumed to be a Gaussian whose mean and variance were linearly related to the amount of light incident on the photocathodes,

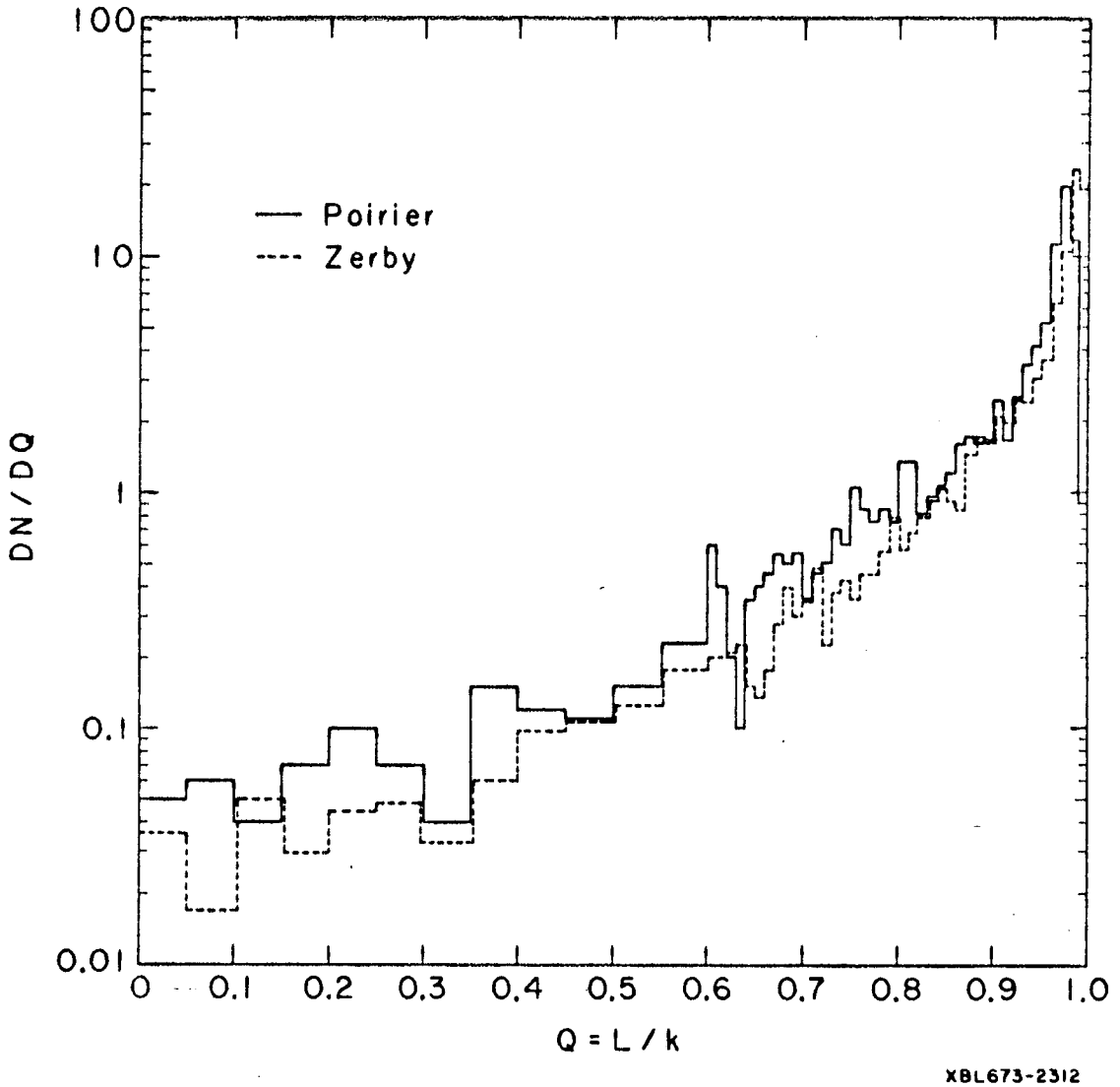

Fig. 9. Results of Monte Carlo calculations of the photon counter response to monoenergetic incident photons; evaluated for incident photon energy of 150 MeV.

$$R_2(L, V) = \frac{1}{sG_2\sqrt{L}\sqrt{2\pi}} \exp -\left[\frac{(V - G_2L)^2}{2s^2G_2{}^2L}\right],$$

where G_2 represents the gain of the photomultiplier system, including the light-collection efficiency. For convenience, we put G_2 equal to unity here, but will include its effect in the overall gain of the system; V and L are dummy variables and may be considered to have the units volts and photons, respectively. This implies that G_2 has the units of volts per photon, and that s^2 has the units of photons. The fractional standard deviation is given by $s/\sqrt{L}$.

The functions $R_1(k, L)$ and $R_2(L, V)$ were folded together by a computer program for various values of the parameter s, and the resulting function

$$R_{12}(k, V, s) = \int R_1(k, L)R_2(L, V)dL$$

was stored on magnetic tape in the form of tables, for use in further calculations. Two evaluations of this function, using the two calculations of $R_1(k, L)$ at k = 130 MeV, are shown in Fig. 10.

A precision electrical pulser was used to measure the shape of the electronics response function; the counting efficiency was determined from measurements made during the experiment and from an evaluation of a sample of the oscilloscope photographs. This efficiency was found to be independent of pulse height, and therefore is a contribution to the energy-independent efficiency, ϵ.

The two remaining parameters (i.e., s, which describes the width of the Gaussian photomultiplier response, and G, which represents the overall gain of the system) were determined by using as calibration data the known spectrum of photons produced by pions stopping in hydrogen. For the spectrum produced by stopping pions we may write an equation similar to Eq. 14,

$$N_i = N_{\pi^0}I_0(i, s, G) + N_\gamma I_3(i, s, G). \qquad (17)$$

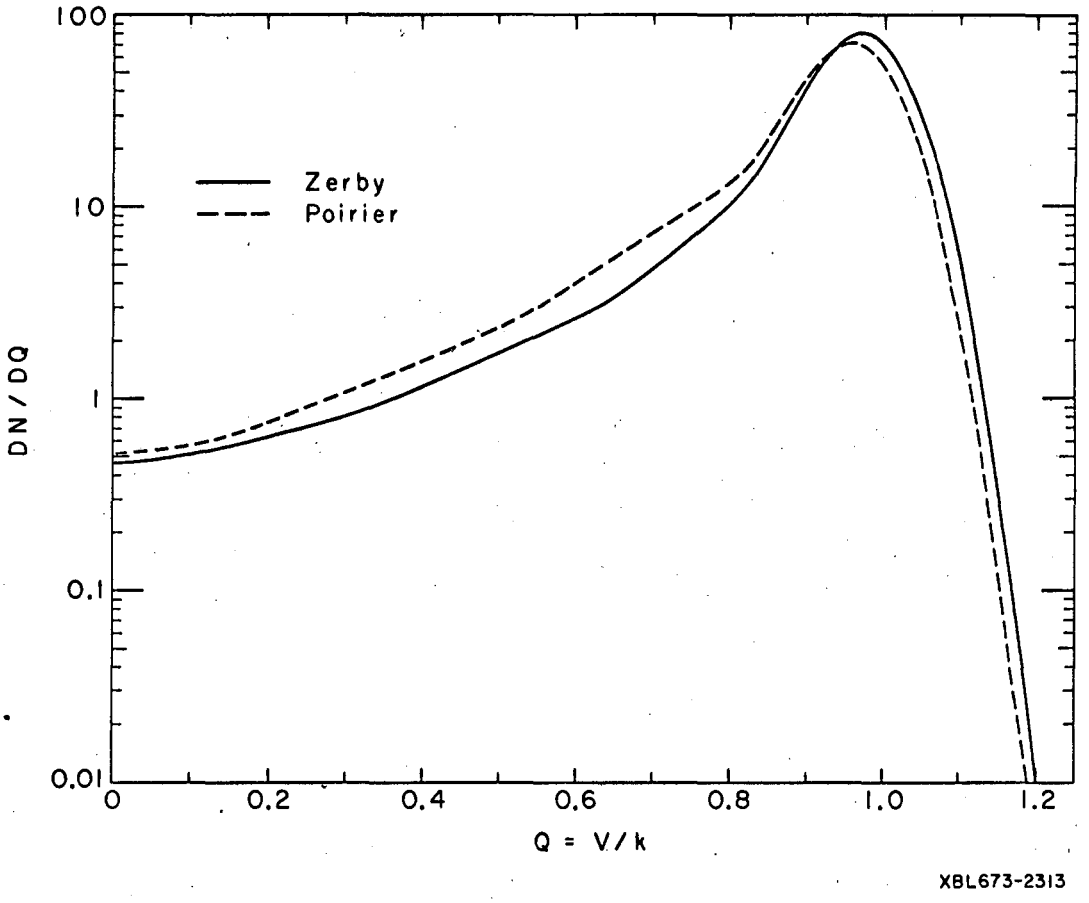

Fig. 10. Photon counter response folded with Gaussian photomultiplier response. Standard deviation of Gaussian = 7% at 130 MeV. Evaluated for incident photon energy of 130 MeV.

In writing Eq. 17 we have used the fact that $\ell = 0$ for stopping pions, and we have indicated explicitly the dependence on s and G; N_γ and N_{π^0} indicate the number of times that reactions 1 and 2, respectively, are produced by the stopping pions; N_{π^0}/N_γ is the Panofsky ratio, P.

Equation 17 was fitted to the experimental data by using a computer program which adjusted N_{π^0}, N_γ, s, and G to minimize χ^2. The measured photon energy spectrum produced by pions stopping in the liquid hydrogen, and the associated fitted curves, are shown in Figs. 11 and 12. The two fits correspond to the use of the two different calculations of the photon counter response. The parameters associated with these best fits are listed in Table III.

Table III. Parameters determined from best fits to stopping pion data.

	Calculations of $R_1(k, L)$	
Characteristics of fit	Poirier	Zerby
S	8.29 ± 0.37	9.07 ± 0.40
G	53.86 ± 0.16	52.97 ± 0.16
χ^2	56.4	49.8
$\mathcal{P}(\chi^2)$	0.05	0.025
Panofsky ratio = N_{π^0}/N_γ	1.72 ± 0.08	1.82 ± 0.08
$\mathcal{P}$ (Panofsky ratio)	0.036	0.001

In Table III, S gives the fractional standard deviation (in percent) of the Gaussian photomultiplier response for an incident photon energy of 130 MeV (corresponding to the energy of monoenergetic photons from reaction 1 at zero incident pion kinetic energy), and G gives the channel number in which the peak corresponding to this energy occurs. The errors given for S and G are the diagonal elements of the error matrix calculated by the fitting program, and are determined by the statistical accuracy of the data and the correctness of the fitted function. The shape of the electronics response function is known with only finite

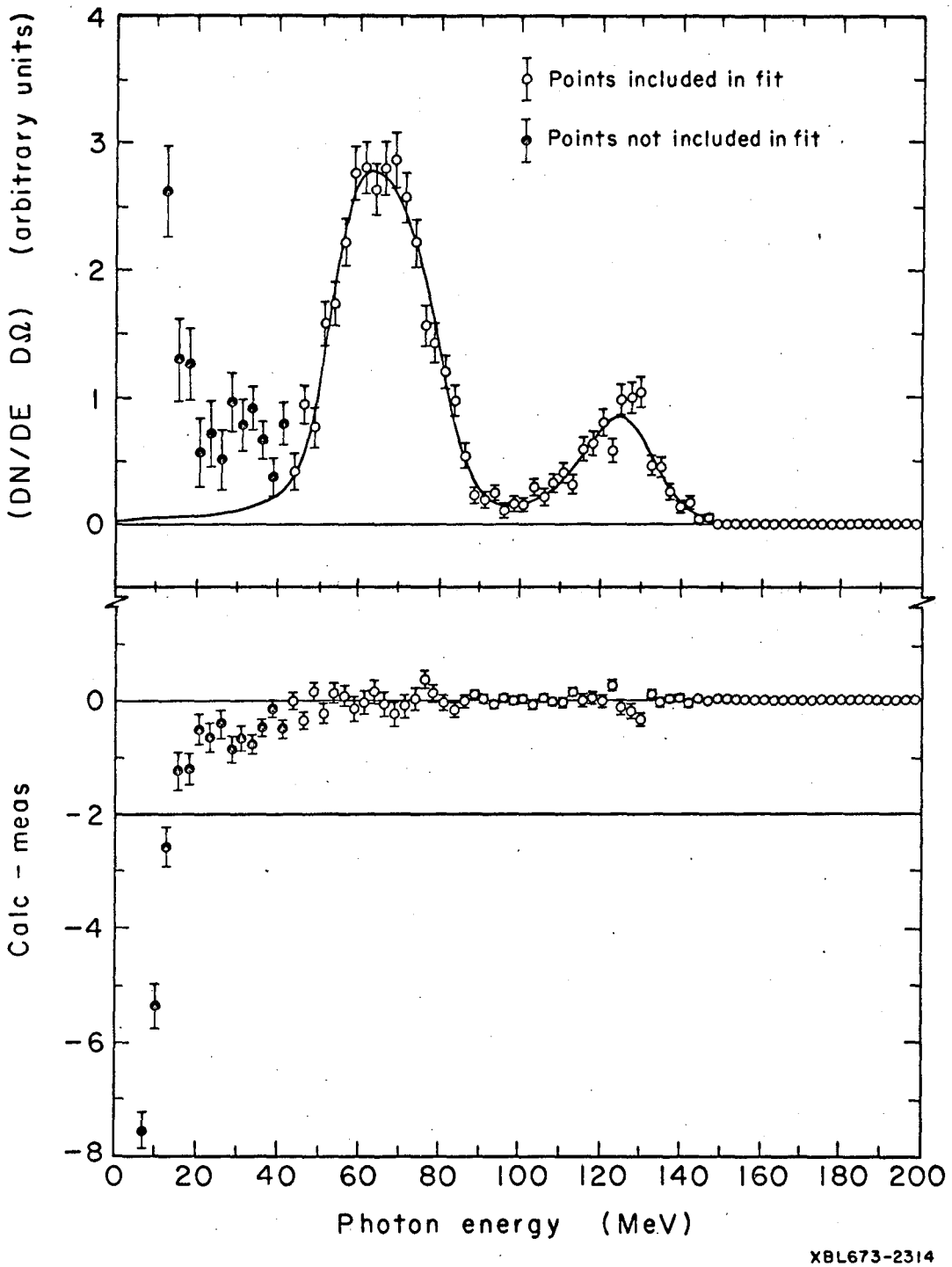

Fig. 11. Fit to stopping pion data using Poirier's calculation of the photon counter response function.

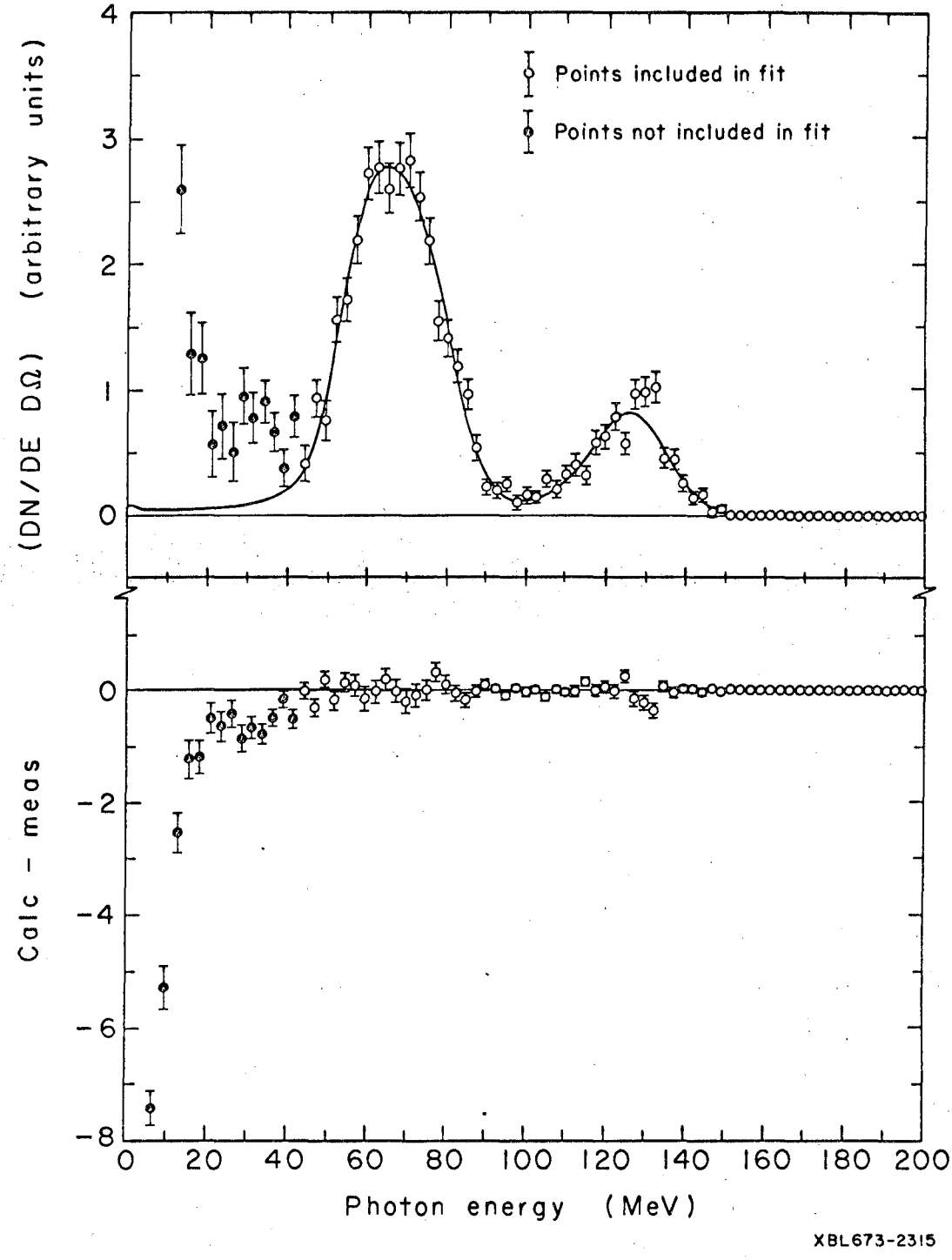

Fig. 12. Fit to stopping pion data using Zerby's calculation of the photon counter response function.

accuracy, and several fits were made to test the sensitivity of the parameters S and G to slight changes in this shape. The variations in S and G caused by this uncertainty were small compared with the statistical errors.

In Table III, $\mathcal{P}(\chi^2)$ is the probability that a value of χ^2 greater than or equal to that obtained experimentally might be obtained because of statistical fluctuations in a measurement of the assumed function. The expression $\mathcal{P}$(Panofsky ratio) is used to indicate a similar probability obtained by making a χ^2 test of the agreement between the value of the Panofsky ratio obtained here and a weighted average of other measurements.[19]

The following comments are relevant to the fits and the parameters determined therefrom. Several points with individual values of χ^2 greater than 4.0 contribute to the large total χ^2. As can be seen from Figs. 11 and 12, the distribution of these points and their deviations from the other data seem to be more indicative of statistical fluctuation than of a systematic deviation from the fitted functions. To say it in another way, there do not appear to be any areas of correlated deviation from the fitted functions. If these points with large values of χ^2 are omitted from the fit, $\mathcal{P}(\chi^2)$ increases to about 0.25 and the values of the parameters are changed by amounts that are small compared with their statistical errors. Thus the fitted curves and the associated values of the parameters may be a more adequate representation of the data than is indicated by the total value of χ^2. However, because we have no a priori reason to suspect these points, we have preferred to present in Table III the values obtained by using all the data.

There are three possible causes for the discrepancy between the value of the Panofsky ratio obtained in this experiment and the average of other recent measurements:

(a) The discrepancy could be the result of statistical fluctuation. As indicated in Table III, the probability that this would occur is $\leq 0.1\%$ for one choice of resolution function, and $\leq 3.6\%$ for the other.

(b) The discrepancy could be the result of a background which was not properly treated in the analysis. There is, in fact, some uncertainty

connected with the subtraction of empty-target background. The energy spectrum of the degraded pion beam was such that only about one third of the incident pions stopped in the hydrogen target. This means that the pions within and emerging from the target had a different energy spectrum, angular distribution, and absolute flux (normalized to the incident flux) depending on whether the target was full or empty. The usual empty-target subtraction, which was used for the data presented in Figs. 11 and 12, depends upon the assumption that the flux of pions through the flask walls and other nearby objects is independent of the presence or absence of hydrogen in the flask. For most experiments, in which both the energy loss and the fraction of the incident beam which interacts in the target are small, this is a good approximation; for the reasons mentioned above we have no good reason to believe that it is a good approximation in the circumstances in which the stopping-pion data were taken. We have made two manipulations of the data to check possible background effects. In one treatment of the data we assumed that the shape of the photon energy spectrum produced by pions interacting in the flask walls and other material was independent of whether the target was full or empty, but that the absolute number of interactions need not have the same proportionality to the incident beam in the two circumstances. As a normalization condition for subtraction of the empty-target data we required that the average number of counts in the subtracted spectrum between 20 and 40 MeV be zero. This normalization was prompted by the fact, noticeable in Figs. 11 and 12, that there is an excess of counts in these channels, where the real counting rate should be close to zero. Because the empty-target spectrum falls off very rapidly with energy, this subtraction had little effect upon the data above 40 MeV, and hence had little effect upon the parameters obtained in the fit. In the second treatment of the data, we attempted to minimize the contribution of any (assumed) low-energy background by increasing the energy below which no data were included in the fit from 40 MeV to 50, 60, and 70 MeV. The parameters of the fit remained consistent with those obtained with a 40-MeV lower limit. We conclude that although there may be uncertainties in the background subtraction they do not appreciably affect the results.

(c) The discrepancy could be the result of using an incorrect response function for the apparatus. The two response functions used in the fitting procedure do yield significantly different values of the Panofsky ratio and χ^2. Furthermore, the original data show that the two functions yield almost identical results for the number of photons produced from π^0's, the major part of the difference between the functions being in the number of photons which the calculations assign to the reaction $\pi^- + p \rightarrow \gamma + n$. Unfortunately, it is impossible to eliminate the possibility that an incorrect response function was used. The only test of the whole analysis system, including the chosen response functions and the apparatus itself, was the data taken with stopping pions, which when analyzed yielded the discrepancy under discussion.

Of the three possibilities, only the third would necessarily lead to incorrect results for the cross-section measurement. The consequences of the discrepancy are discussed further in Sec. IV.

The channel-number distributions described in Eqs. 15 and 16 were calculated for both the response functions whose characteristics are given in Table III.

The set of parameters, A_j and $d\sigma_{\gamma,1}/d\Omega^*$, that best fitted the experimental data was calculated with a program which adjusted the parameters to minimize χ^2, where

$$\chi^2 = \sum_i \left[\frac{N_i^{meas} - N_i^{calc}\left(A_j, \frac{d\sigma_{\gamma,1}}{d\Omega^*}\right)}{\Delta N_i} \right]^2 . \qquad (18)$$

In addition to the best set of parameters and the associated value of χ^2, the program also calculated the error matrix[22] of the parameter.

In Eq. 18, $N_i^{calc}(A_j, d\sigma_{\gamma,1}/d\Omega^*)$ was calculated from Eq. 14, and N_i^{meas} and ΔN_i were obtained from the experimental data by the relations

$$N_i^{meas} = N_i^{full} - \left(\frac{N_\pi^{full}}{N_\pi^{mt}} \right) N_i^{mt} ,$$

$$\Delta N_i = \left[\left(N_i^{full} + 1 \right) + \left(\frac{N_\pi^{full}}{N_\pi^{mt}} \right)^2 \left(N_i^{mt} + 1 \right) \right]^{1/2} .$$

In these expressions, N_i^{full} and N_i^{mt} represent the channel-by-channel sum of all experimental pulse-height-analyzer distributions taken with the target full and empty, respectively; N_π^{full} and N_π^{mt} represent the total number of pions passing through the target while these distributions were being measured. No separate accidentals correction was necessary because both the rate of accidentals per incident pion and the shape of the accidentals pulse-height spectrum were independent of whether the target was full or empty; hence this effect is accounted for in the simple (full-mt) subtraction. In making the (full-mt) subtraction it is also necessary to correct for the residual hydrogen gas which remains in the target during the "mt" runs. This may be done by replacing ρ in Eq. 14 by

$$\rho_{eff} = \rho_{full} - \rho_{mt} .$$

The value of ρ_{eff} used in this experiment was

$$\rho_{eff} = (70.0 \pm 0.4) g/\ell .$$

B. Oscilloscope Photographs

The oscilloscope photographs were measured on a digitized measuring projector which transferred the x, y coordinates of selected spots on the film onto an IBM card. Measurements of timing, or pulse height, or both, were made on the pulses of interest. A timing measurement consisted of measuring the x, y coordinates of the half height of the leading edge of the pulse, and a pulse-height measurement consisted of a series of points defining the base line and the peak height of the pulse. Computer programs were written to transform these measurements into the quantities of interest (relative timing and pulse height) and to make one- and two-dimensional histograms of the results.

Our chief interest in the results from the photographs was to check that the efficiency of the $C_4(C_3\gamma)$ coincidence was independent of the overall pulse height in the photon counter. We found that the time spread between the C_3 and γ signals was about 5 nsec and that it was approximately centered within the 20-nsec coincidence time of C_4.

IV. RESULTS

The results obtained by fitting the calculated spectra to the experimental data are given in Table IV. Figures 13 and 14 show comparisons between the data and the fitted functions. The errors listed in Table IV are the standard deviations calculated by the fitting program and are based on the statistical errors in the data. These errors are not appreciably increased when the uncertainties in the response functions are taken into account.

It happens that because of the placement of the photon counter, the parameter A_1 appears in the fit multiplied by a small coefficient, and as a consequence is poorly determined by this experiment. Fixing A_1 at a value obtained by interpolation between other nearby measurements makes it possible to reduce the errors on the other parameters. The values of the other parameters are insensitive to the choice of A_1 because of its small coefficient. The data from which A_1 was determined are shown in Fig. 15.

The correlation matrix C_{ij} given in Table IV is related to the error matrix ϵ_{ij} by

$$C_{ij} = \epsilon_{ij}/\sigma_i\sigma_j ,$$

where σ_i is the standard deviation of the ith parameter.

The excess in the data below 20 MeV, exhibited in Figs. 13 and 14, is believed to be caused by a rapid rise in the unsubtracted data in this region coupled with a small difference in average gain during the full and empty running conditions. The full, empty, and subtracted data (normalized to the incident flux) are shown in Fig. 16. Several fits were made to test the sensitivity of the parameters to the amount of low-energy data included in the fit. No significant variation in the parameters was observed for a wide range of low-energy cutoffs.

In addition to the errors depending upon the statistical accuracy of the pulse-height-analyzer spectra, there is also an overall error associated with multiplicative factors such as the density and thickness of the hydrogen target, the total number of incident pions, and the energy-independent efficiency of the apparatus. These factors and associated errors are given in Table V.

Table IV. Results of fitting procedure.

Parameter (mb/sr)	Calculation of photon counter response function: Poirier	Zerby
A_0	0.682 ± 0.015	0.680 ± 0.014
A_1	(Fixed at -0.8)	
A_2	0.531 ± 0.054	0.565 ± 0.052
$\frac{d\sigma_{\gamma,1}}{d\Omega^*}$ ($\theta^* \approx 90$ deg)	0.0515 ± 0.0062	0.0476 ± 0.0058

Correlation matrix for fit using Poirier's calculation, $\chi^2 = 41.6$, $\mathcal{P}(\chi^2) = 0.4$.

	A_0	A_2	$\frac{d\sigma_{\gamma,1}}{d\Omega^*}$
A_0	1	0.81	-0.09
A_2		1	0.40
$\frac{d\sigma_{\gamma,1}}{d\Omega^*}$			1

Correlation matrix for fit using Zerby's calculation, $\chi^2 = 41.6$, $\mathcal{P}(\chi^2) = 0.4$.

	A_0	A_2	$\frac{d\sigma_{\gamma,1}}{d\Omega^*}$
A_0	1	0.82	0.03
A_2		1	0.39
$\frac{d\sigma_{\gamma,1}}{d\Omega^*}$			1

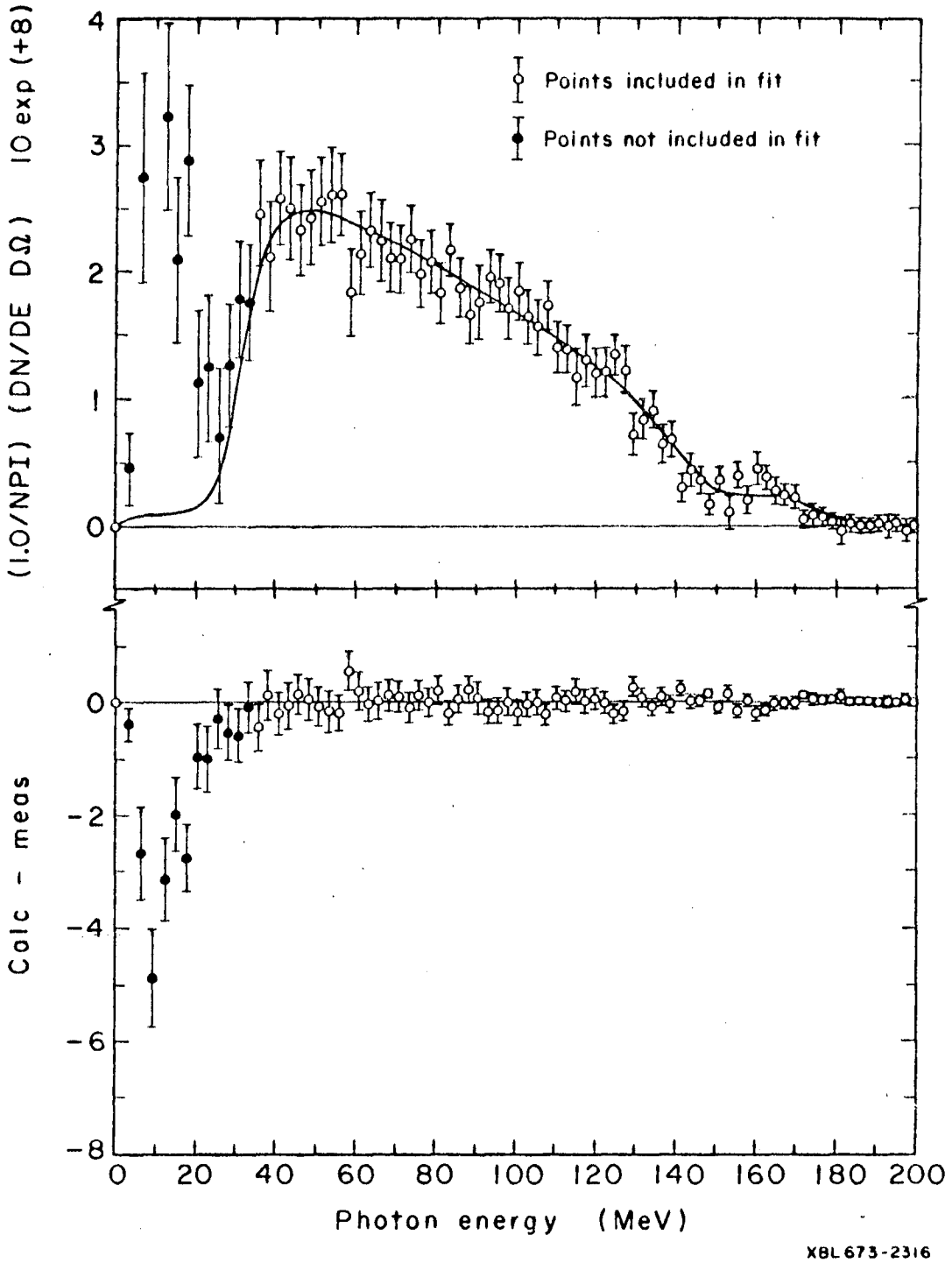

Fig. 13. Fit to the experimental data using Poirier's calculation of the photon counter response function.

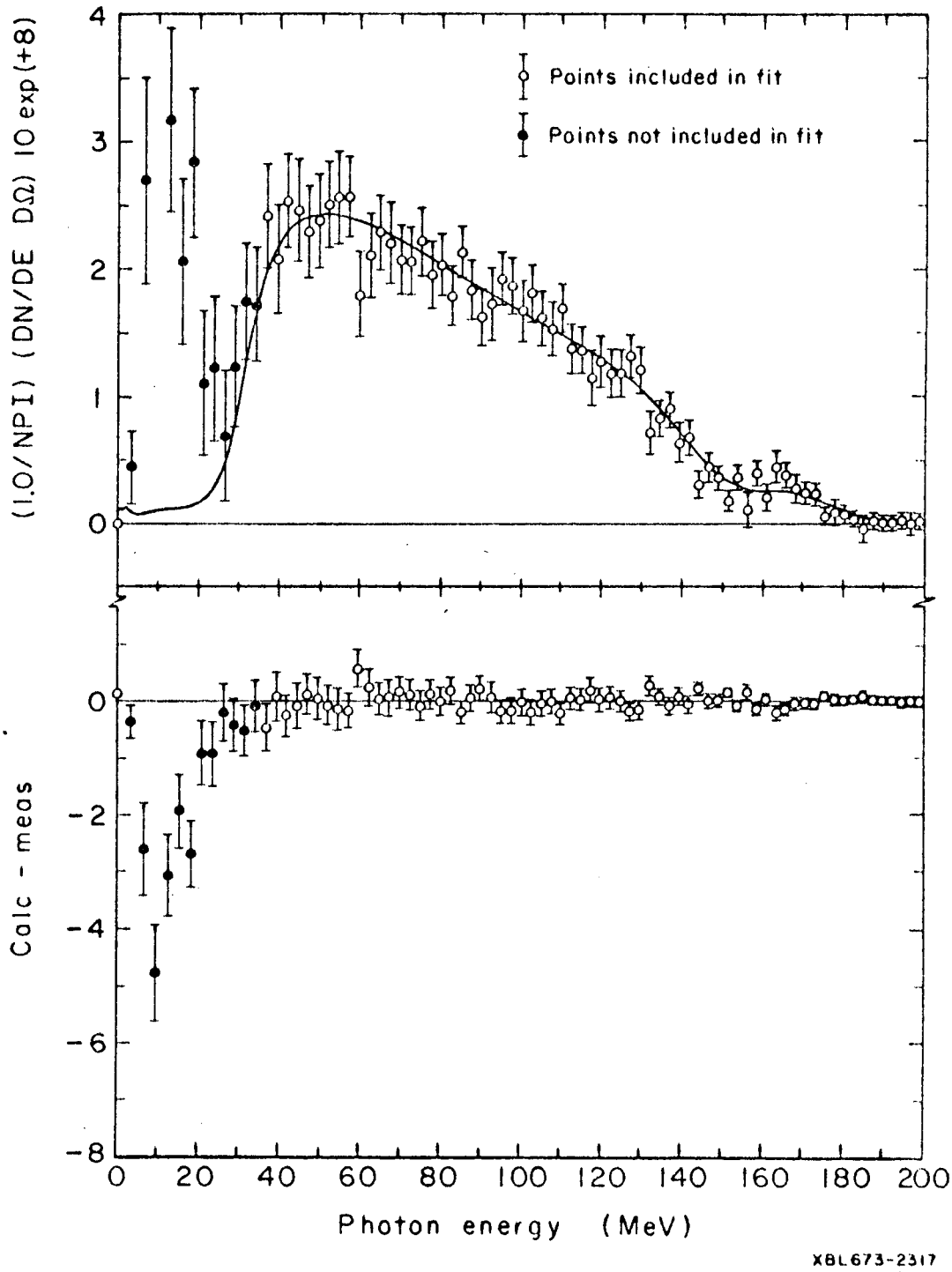

Fig. 14. Fit to the experimental data using Zerby's calculation of the photon counter response function.

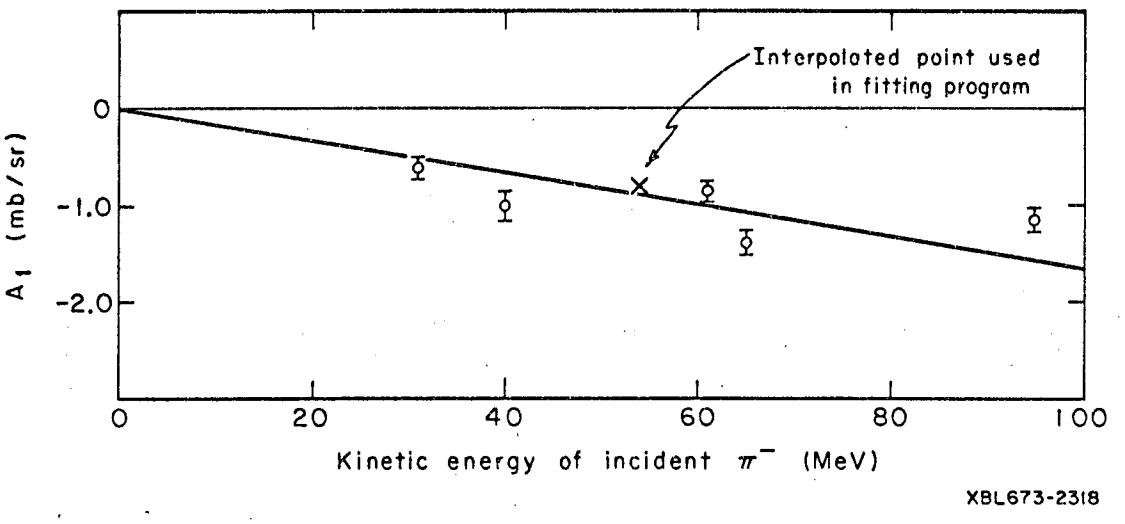

Fig. 15. Available data on the coefficient A_1 in the Legendre series expansion of the charge-exchange c.m. differential cross section, showing how the value used in the fitting procedure was chosen.

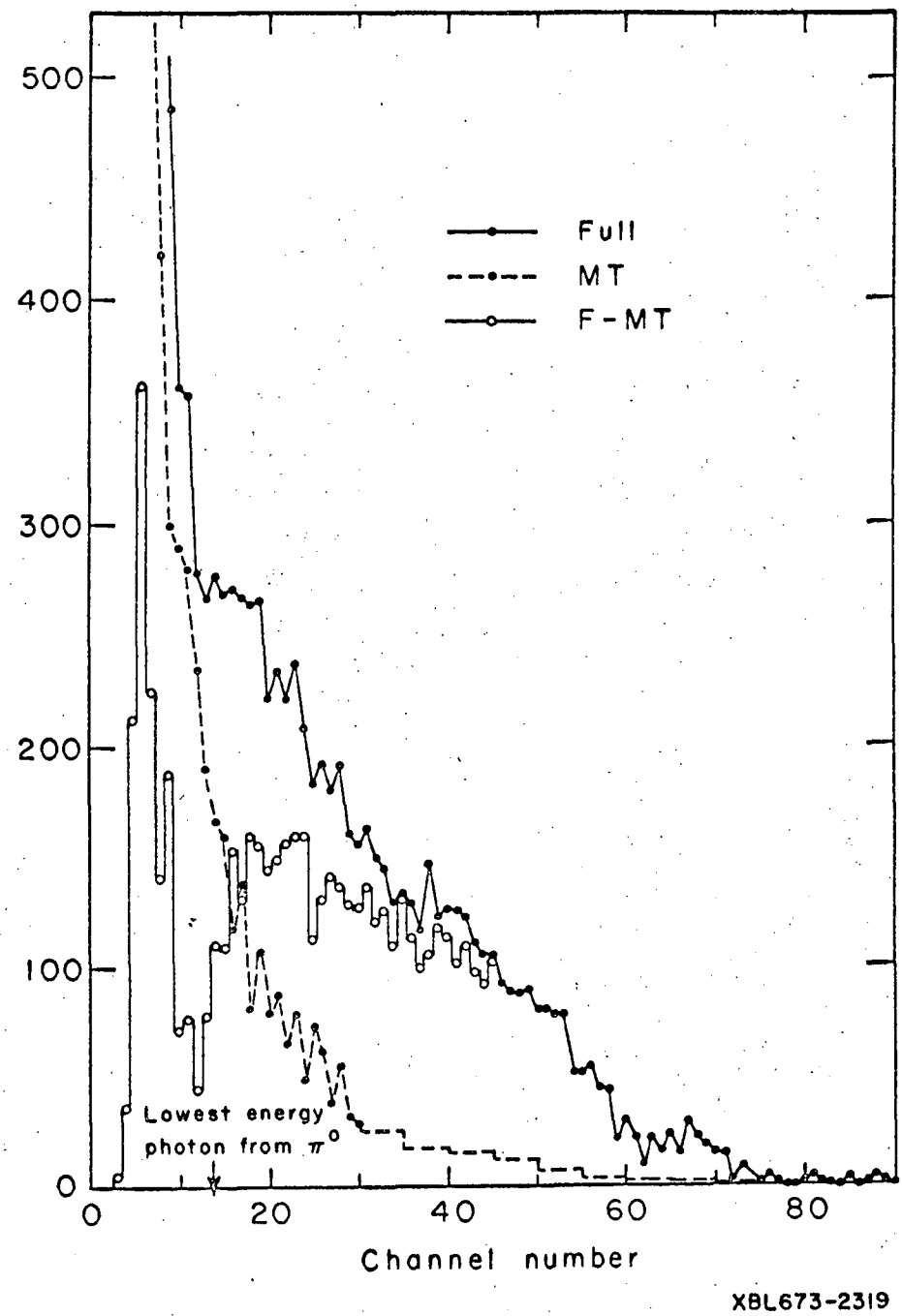

Fig. 16. Full, empty, and subtracted data (normalized to incident flux) showing rapid rise below channel 10 (approximately 20 MeV).

Table V. Multiplicative factors and errors.

Factor	Value	% Error
Hydrogen density	70.0 g/ℓ	0.5
(Target thickness × solid angle)	0.0174 in. sr.	4.0
N_π	2.7×10^9	1.5
Overall efficiency		
electronics	0.865	3.0
scattering out of γ's	0.99	0.5
anti by neutron or other γ	0.99	1.0
Overall error		5.4

We combine the overall error given in Table V incoherently with the standard deviations given in Table IV to obtain the total error of the parameters. The values of the parameters and the total errors are given in Table VI.

Table VI. Parameters and total errors.

Parameter (mb/sr)	Calculation of photon counter response function	
	Poirier	Zerby
A_0	0.68 ± 0.04	0.68 ± 0.05
A_1	Not determined by this experiment	
A_2	0.53 ± 0.06	0.56 ± 0.06
$\frac{d\sigma_{\gamma,1}}{d\Omega^*}(\theta^* \approx 90°)$	0.0515 ± 0.0068	0.0476 ± 0.059

We now return to the discussion of our discrepant value for the Panofsky ratio and the problem of the two response functions. As mentioned earlier, in Sec. III, the discrepant value for the Panofsky ratio could be caused by using an incorrect response function for the photon counter, and this is the only possibility that could lead to incorrect values for the cross sections given above. Because we have made all calculations using two response functions, we have adopted the following procedure.

For our best estimate of the parameters we have chosen those obtained when using the photon counter response function calculated by Poirier. This choice was made because in fitting the stopping pion data this response function yielded both a higher $\mathcal{P}(\chi^2)$ and a less discrepant value of the Panofsky ratio.

To assign systematic errors due to uncertainties in the response function we have chosen to add to the random error of each parameter a systematic error equal to the difference in the two values of that parameter calculated from the two response functions. Although this choice is rather arbitrary, this number is the only available measure of the sensitivity of the results to changes in response function.

The best estimates of the parameters and their errors are therefore

A_0	(0.68 ± 0.04) mb/sr,
A_1	not determined by this experiment,
A_2	(0.53 ± 0.09) mb/sr,
$\frac{d\sigma_{\gamma,1}}{d\Omega^*}(\theta^* \approx 90 \text{ deg})$	(51.5 ± 10.7) .

Combining expressions 1 and 5 with our result for $\frac{d\sigma_{\gamma,1}}{d\Omega^*}(\theta^* \approx 90 \text{ deg})$, we obtain

$$a_0^- = (15.4 \pm 3.2)\ \mu\text{b/sr}$$

at an equivalent incident photon energy of 202 MeV.

V. CONCLUSIONS

As mentioned in Sec. I, the results of this experiment may be compared with the π^- photoproduction data through the principle of detailed balance, and with the charge-exchange data through the Panofsky ratio. For the latter comparison, a convenient common ground is the S-wave scattering length difference $(a_1 - a_3)$. We now proceed to discuss these comparisons.

By comparing our result for a_0^- with the results obtained from the deuterium data we may test, within the accuracy of the respective experiments, the joint validity of the deuterium corrections and the principle of detailed balance. This comparison is shown in Fig. 17. The datum of Gatti et al.[23] comes from a measurement of the radiative capture cross section and not from a photoproduction experiment. Both the datum from Swanson et al.[24] and the data from Yoon[25] are obtained from experiments performed in deuterium bubble chambers. These experiments permit the use of a Chew-Low extrapolation technique[26] to get the cross section for photoproduction on free neutrons. The curves were calculated from the CGLN theory[27] of photoproduction using $N^- = 0$; they are labeled with the values of the pion-nucleon coupling constant f^2 used in the calculation. Here $f^2 = 0.081 \pm 0.003$ is the accepted value obtained from charged pion-nucleon scattering; $f^2 = 0.073 \pm 0.003$ is the value obtained by Yoon in a fit of the CGLN theory to his data. (It has been suggested[28] that the photoproduction cross section may be in error due to difficulties in calibrating the instruments used to measure the absolute photon flux. However, we note that a recent experiment on π^+ photoproduction[29] yields a value of $f^2 = 0.079 \pm 0.003$, using the CGLN theory and assuming $R_{+/-} = 1.3$. This π^+ experiment used the same photon beam-monitoring equipment as used by Yoon.) We conclude that there does not appear to be any disagreement between our value of a_0^-, obtained from the radiative capture reaction, and those values obtained from the deuterium data. Primarily because of the low accuracy of the datum from this experiment, this does not prove to be a stringent test of the principles of detailed balance. We also note that the data do not seem to be in

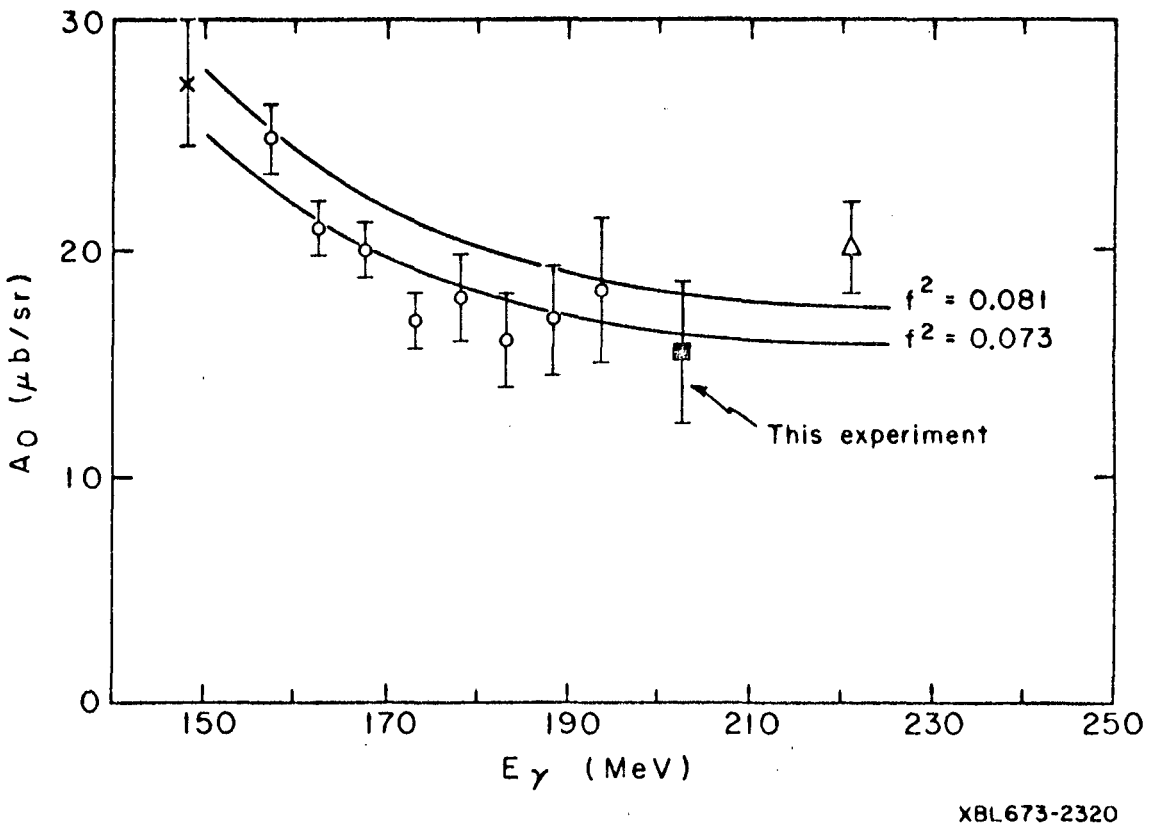

Fig. 17. Values of the π^- photoproduction coefficient a_0^-:

- This experiment
- Yoon (Ref. 25)
- Swanson et al. (Ref. 24)
- Gatti et al. (Ref. 23)

The curves are calculated from the dispersion theory of CGLN (Ref. 27), using the values of f^2 on the graph.

agreement with the CGLN theory using the accepted value for the coupling constant. Again because of its large error, our result does not lend much weight to this trend.

In order to compare the radiative capture results with the charge-exchange data one must extrapolate to Q = 0. Because an extrapolation to zero of our single datum would be of little weight, and because this datum agrees so well with the data and the CGLN fit of Yoon, as shown in Fig. 17, we have chosen to discuss the threshold value of a_0^- given by this fit. Yoon obtains $a_0^-(Q=0) = (26.0 \pm 1.0)$ μb/sr. From expression 6 we may then calculate $(a_1 - a_3) = 0.241 \pm 0.010$. A similar calculation based on the datum of Swanson et al.[24] yields $(a_1 - a_3) = (0.247 \pm 0.013)$. These results, together with other recent evaluations of the scattering length difference, appear in Table VII.

Table VII. Recent evaluations of s-wave scattering length difference $(a_1 - a_3)$.

Type of data used in evaluation	Reference	$a_1 - a_3$
Photoproduction data and Panofsky ratio	Yoon, 25	0.241 ± 0.010
	Swanson et al., 24	0.247 ± 0.013
	Donnachie and Shaw, 31	0.254 ± 0.013[a]
Charge-exchange data	Hamilton, 30	0.266
	Donald et al., 32	0.291 ± 0.013
Charged pion–nucleon scattering data	Höhler and Baacke, 33	0.292 ± 0.011
	Samaranayake and Woolcock, 34	0.292 ± 0.020
	Hamilton, 30	0.271 ± 0.007 0.265 ± 0.007[b]

a. The result of Donnachie and Shaw is not obtained by application of CGLN theory to the π^- photoproduction data.

b. This number represents Hamilton's estimate of the "charge independent" scattering length difference (i.e., that which should be used for charge exchange).

The entries in this table have been divided into categories indicating the type of data on which the evaluations are based.

It is evident from Table VII that there is no consensus on a unique value for $(a_1 - a_3)$. Hamilton[30] believes that the charge-exchange and elastic-scattering data can be reconciled at a value of $(a_1 - a_3) = 0.266$. This is about one or two standard deviations away from the values obtained from photoproduction data and the Panofsky ratio. The other evaluations based on scattering data, in both charged scattering and charge-exchange scattering, also achieve agreement, at $(a_1 - a_3) = 0.292$, but this is four or five standard deviations away from the photoproduction value. It is perhaps significant that Hamilton's analysis of the charged data is based on experiments done at energies below 41.5 MeV, while the other analyses are based on dispersion integrals of the $\pi^{\pm}$ total cross sections over the energy range $0 \rightarrow \infty$. Höhler[33] has suggested that in order to resolve the difficulties it may be necessary to re-examine the methods used at low energies for making Coulomb corrections and for taking into account the mass difference between charged and neutral pions.

Our value of A_0 is given in Fig. 18 along with other charge-exchange data and some curves calculated for various values of $(a_1 - a_3)$. The calculations are based on the parameterization by Hamilton and Woolcock,[10] and use the values of P-wave phase shifts and other parameters given in their paper. It is evident from the figure that the general trend of the data is considerably higher than the curve based on the value of $(a_1 - a_3)$ obtained from photoproduction data and the Panofsky ratio.

In Fig. 19 our value of A_2 is shown along with other available data and a curve calculated as in Fig. 17. Only one curve appears, since A_2 depends only upon the P-wave phase shift.

It appears that there remains something to be explained in the field of S-wave pion physics. There is still disagreement among the values of $(a_1 - a_3)$ determined from different types of data, and even some disagreement in values obtained from the same data. There is also the discrepancy between the value of the coupling constant f^2

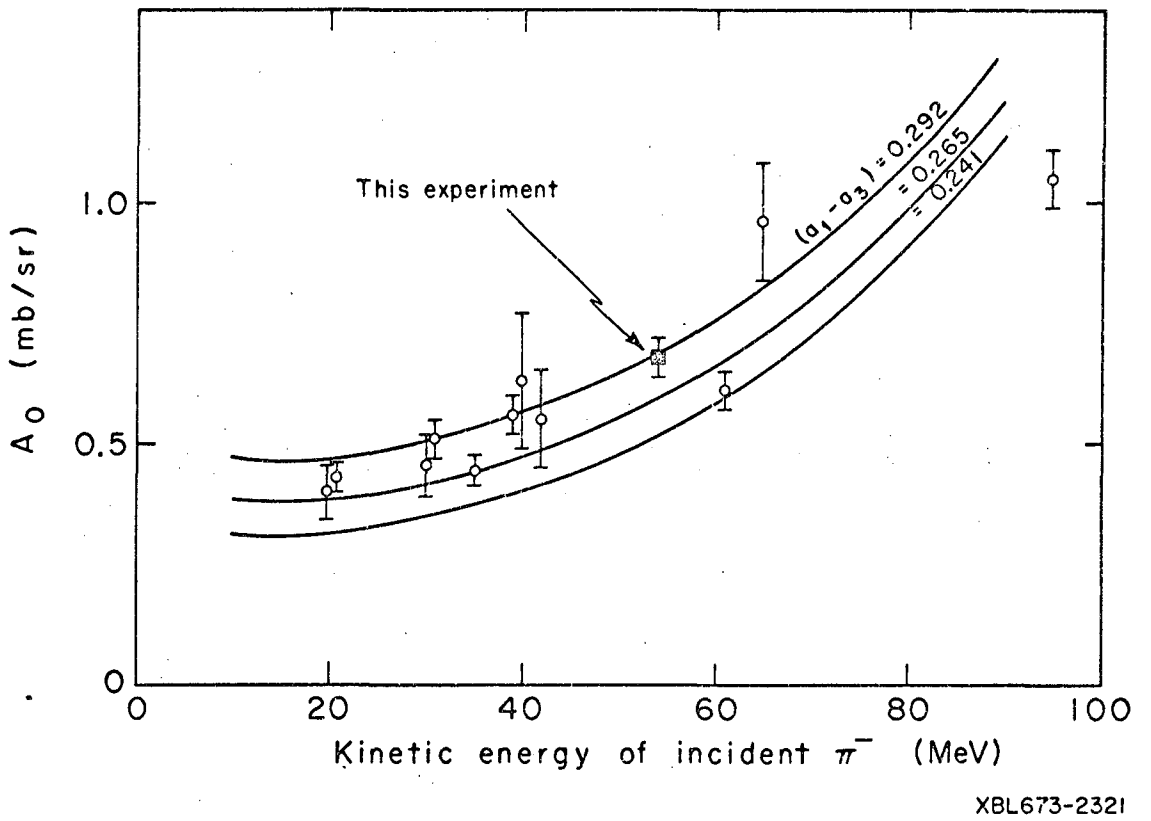

Fig. 18. Measurements of the coefficient A_0 in the Legendre series expansion of the charge-exchange c.m. angular distribution. The data shown were obtained from a list given in Ref. 35. Recent measurements from Refs. 32 and 36 were added. The curves were calculated from Hamilton and Woolcock's parameterization of the S- and P-wave phase shifts (Ref. 10). Values of $(a_1 - a_3)$ were chosen from Table VII.

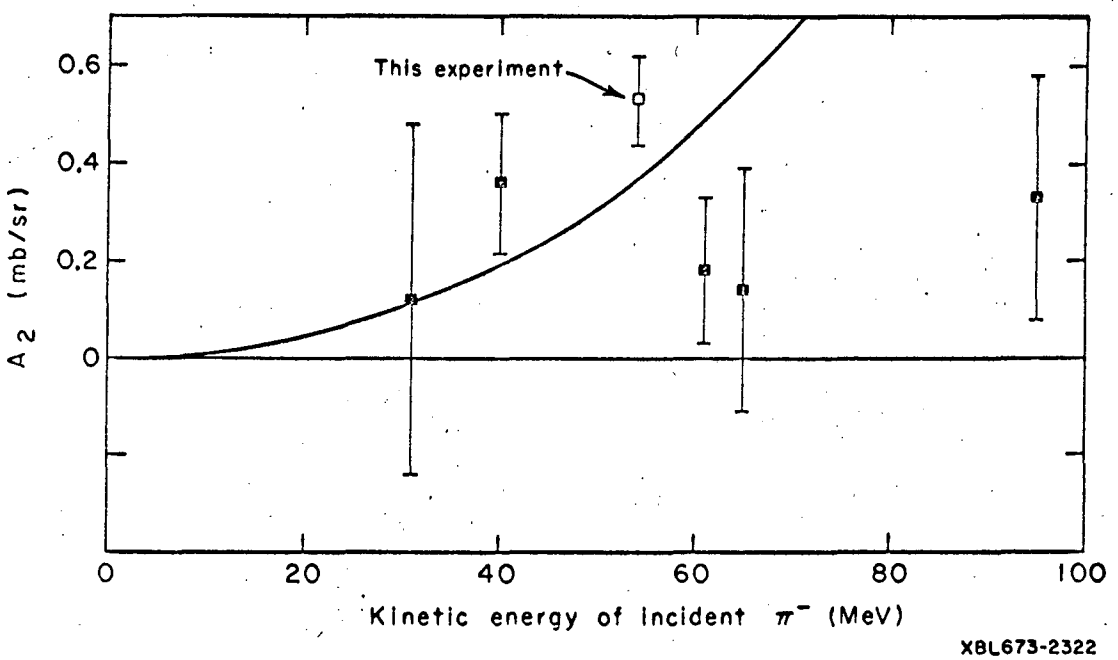

Fig. 19. Measurements of the coefficient A_2 in the Legendre series expansion of the charge-exchange c.m. angular distribution. The data were obtained from a list given in Ref. 35. The curve was calculated from Hamilton and Woolcock's parameterization of the P-wave phase shifts (Ref. 10).

obtained from π^- photoproduction, and the value obtained both from charged pion-nucleon scattering and from π^+ photoproduction. This experiment has indicated, although with low significance, that there is no discrepancy between present data and the principle of detailed balance.

ACKNOWLEDGMENTS

I wish to thank Dr. John A. Poirier for the guidance which he has provided during our association, for suggesting this experiment, and for his essential assistance during the experimental program. My thanks also go to my colleague, Dr. William C. Bowman, who shared the effort of designing and assembling the apparatus, and the work of collecting the data. Special thanks are due Dr. Morris Pripstein for his excellent design of the pion beam.

The support, direction, and encouragement provided by Dr. R. W. Kenney and by Dr. B. J. Moyer are gratefully acknowledged.

I wish to express my appreciation to the people of the various Laboratory support groups who have contributed directly to the experiment; it is unfortunately not possible to name them all here.

I also wish to thank Dr. Clayton D. Zerby, Fred C. Maienschein, and H. S. Moran for providing me with their calculations of the shower behavior in the total absorption counter.

This work was done under auspices of the U. S. Atomic Energy Commission.

REFERENCES

1. H. L. Anderson and E. Fermi, Phys. Rev. 86, 794 (1952).
2. W. S. C. Williams, An Introduction to Elementary Particles (Academic Press, New York, 1961), Sec. 5.6.
3. G. Puppi, in Proc. Ann. Rochester Conf. on High Energy Physics, 1958.
4. A. M. Baldin, Nuovo Cimento 8, 569 (1958).
5. J. M. Cassele, G. Fidecaro, A. M. Wetherell, and J. R. Wormald, Proc. Phys. Soc. (London) A70, 405 (1957).
6. M. Beneventano, G. Bernardini, D. Carlson-Lee, and G. Stoppini, Nuovo Cimento, Ser. 10, 4, 323 (1956).
7. J. Orear, Phys. Rev. 100, 288 (1955).
8. M. Cini, R. Gatto, E. L. Goldwasser, and M. A. Ruderman, Nuovo Cimento, Ser. 10, 4, 323 (1956).
9. J. Hamilton and W. S. Woolcock, Phys. Rev. 118, 291 (1960).
10. J. Hamilton and W. S. Woolcock, Rev. Mod. Phys. 35, 737 (1963).
11. The characteristics of the beam were calculated by using the program OPTIK, described in Thomas J. Devlin, OPTIK: an IBM 709 Computing Program for the Optics of High Energy Particle Beams, Lawrence Radiation Laboratory Report UCRL-9727, Sept. 1961 (unpublished).
12. Arthur E. Bjerke, Quentin A. Kerns, and Thomas A. Nunamaker, Time Resolution of a Scintillation Counter System, Lawrence Radiation Laboratory Report UCRL-9976, Feb. 1962 (unpublished).
13. William C. Bowman, Jim B. Carroll, and John A. Poirier, Total-Absorption Scintillation Counter for High-Energy Photons, Rev. Sci. Instr. 33, 7 (1962).
14. A. Kantz and R. Hofstadter, Nucleonics 12, 3, 36 (1954).
15. Designed by Cordon R. Kerns, (Lawrence Radiation Laboratory), private communication.
16. W. J. Kernan, Charge Exchange Scattering of Negative Pions at 150 MeV, Phys. Rev. 119, 1092 (1960).
17. John A. Poirier (University of Notre Dame, Notre Dame, Indiana), private communication.

18. C. D. Zerby and H. S. Moran, Studies of the Longitudinal Development of High Energy Electron-Photon Cascade Showers in Copper, Oak Ridge National Laboratory Report ORNL-3329, 1962 (unpublished).
19. The value used for the weighted average of the Panofsky ratio was 1.53 ± 0.04. The data used in calculating this weighted average are listed in Ref. 20. Referring to these data, measurements (a) and (c) were omitted and the error measurement (j) was increased to 0.04. A recent measurement by Ryan (Ref. 21) was also included.
20. V. T. Cocconi, T. Tazzini, G. Fidicaro, M. Legros, N. H. Lipman, and A. W. Merrison, Nuovo Cimento 22, 494 (1961).
21. J. W. Ryan, Phys. Rev. 130, 1554 (1963).
22. See, for example, the discussion of the error matrix in Peter Cziffra and Michael J. Moravcsik, A Practical Guide to the Method of Least Squares, Lawrence Radiation Laboratory Report UCRL-8523 Rev., June 1959 (unpublished).
23. G. Gatti, P. Hillman, W. C. Middelkoop, T. Yamagata, and E. Zovottini, Phys. Rev. Letters 6, 706 (1961).
24. W. P. Swanson, D. P. Gates, T. L. Jenkins, and R. W. Kenney, Phys. Rev. 137B, 1188 (1964).
25. Taek-Soon Yoon, Photoproduction of Charged Pions From Deuterium near Threshold (Ph. D. Thesis), University of Illinois, May 1964 (unpublished).
26. G. F. Chew and F. E. Low, Phys. Rev. 113, 1640 (1959).
27. G. F. Chew, F. Goldberger, F. E. Low, and Y. Nambu, Phys. Rev. 106, 1345 (1957).
28. R. W. Kenney (Lawrence Radiation Laboratory), private communication.
29. James D. Simpson, Photoproduction of Positive Pions Near Threshold in Hydrogen (Ph. D. Thesis), University of Illinois, June 1964 (unpublished).
30. J. Hamilton, Pion-Nucleon Scattering and Conservation Laws, Phys. Letters 20, 6 (1966).
31. A. Donnachie and G. Shaw, Low Energy Photoproduction, SU(6), and the Panofsky ratio (to be published).

32. R. A. Donald, W. H. Evans, W. Hart, P. Mason, D. E. Plane, and J. Reid, Proc. Phys. Soc. (London) 87, 445 (1966).

33. G. Höhler and J. Baacke, The Parameters of Low Energy Pion Physics (to be published).

34. V. K. Samaranayake and W. S. Woolcock, New Determination of the Pion-Nucleon Coupling Constant and S-Wave Scattering Lengths, Phys. Rev. Letters 15, 24 (1965).

35. K. Miyaki, K. F. Kinsey, and D. E. Knapp, University of Rochester Department of Physics and Astronomy Report NYO-9545 (unpublished).

36. D. C. Cundy, R. A. Donald, W. H. Evans, W. Hart, P. Mason, D. E. Plane, J. R. Smith, and J. G. Thomas, Proc. Phys. Soc. (London) 85, 257 (1965).